Astronomy & Astrophysics manuscript no. papTiO2Nuc˙corrHDK˙editedGL
November 12, 2014

Dust in brown dwarfs and extra-solar planets

IV. Assessing TiO_2 and SiO nucleation for cloud formation modelling

G. Lee[1], Ch. Helling[1], H. Giles[1], and S. T. Bromley[2,3]

[1] SUPA, School of Physics and Astronomy, University of St. Andrews, North Haugh, St. Andrews, KY16 9SS, United Kingdom
email: ch80@st-and.ac.uk
[2] Departament de Quimica Fisica and IQTCUB, Universitat de Barcelona, Marti i Franques 1, E-08028 Barcelona, Spain
[3] Institucio Catalana de Recerca i Estudis Avancats (ICREA), E-08010 Barcelona, Spain

Accepted 2012 ?, Received 2012 ?, in original from November 12, 2014

ABSTRACT

Context. Clouds form in atmospheres of brown dwarfs and planets. The cloud particle formation processes, seed formation and growth/evaporation are very similar to the dust formation process studied in circumstellar shells of AGB stars and in supernovae. Cloud formation modelling in substellar objects requires gravitational settling and element replenishment in addition to element depletion. All processes depend on the local conditions, and a simultaneous treatment is required.
Aims. We apply new material data in order to assess our cloud formation model results regarding the treatment of the formation of condensation seeds. We look again at the question of the primary nucleation species in view of new $(TiO_2)_N$-cluster data and new SiO vapour pressure data.
Methods. We applied the density functional theory (B3LYP, 6-311G(d)) using the computational chemistry package Gaussian 09 to derive updated thermodynamical data for $(TiO_2)_N$ clusters as input for our TiO_2 seed formation model. We tested different nucleation treatments and their effect on the overall cloud structure by solving a system of dust moment equations and element conservation for a prescribed Drift-Phoenix atmosphere structure.
Results. Updated Gibbs free energies for the $(TiO_2)_N$ clusters are presented, as well as a slightly temperature dependent surface tension for T=500 . . . 2000K with an average value of σ_∞ = 480.6 erg cm^{-2}. The TiO_2 seed formation rate changes only slightly with the updated cluster data. A considerably larger effect on the rate of seed formation, and hence on grain size and dust number density, results from a switch to SiO nucleation. The question about the most efficient nucleation species can only be answered if all dust/cloud formation processes and their feedback are taken into account. Despite the higher abundance of SiO over TiO_2 in the gas phase, TiO_2 remains considerably more efficient at forming condensation seeds by homogeneous nucleation. The paper discusses the effect on the cloud structure in more detail.

Key words. astrochemistry - Methods: numerical - Stars: atmospheres - Stars: low-mass, brown dwarfs - Stars: AGB

1. Introduction

Brown dwarfs have long been known to form dust in atmospheres and recent detections demonstrate their observational comparability to giant exoplanets like 2M0355 and 2M1207b (see Faherty et al. 2013). Transit spectroscopy observations of exoplanets suggest the presence of haze layers in HD 189733b (Lecavelier Des Etangs et al. 2008, Sing et al. 2011, Pont et al. 2013), GJ 1214b (Miller-Ricci Kempton et al. 2012), WASP-12b (Copperwheat et al. 2013, Sing et al. 2013) and CoRot-1b (Schlawin et al. 2014). The formation of cloud particles affects the observed spectrum of all of these objects by depleting the local gas phase and by providing an additional opacity source. The interpretation of such observations requires understanding and modelling of the cloud formation processes. We will demonstrate that the processes involved in cloud formation cannot be treated independently *a priori*, instead their interacting feedback needs to be considered. This includes formation of new particles (nucleation), the growth and evaporation of existing particles, their gravitational settling (or other large-scale relative motions), convective mixing, and element depletion.

Nucleation rates of various chemical species are important for the formation of cloud layers, but also for modelling the element enrichment by winds of AGB stars and supernovae. In oxygen rich atmospheres TiO_2 molecules have been identified as important players in seed formation due to its chemically reactive sites. In addition, the stability of TiO_2[s] has been proven experimentally (Demyk et al. 2004) which further supports it as a likely candidate for nucleation seeds.

Previous work on $(TiO_2)_N$ clusters as precursors for condensation seeds, that form through a step-wise increase of cluster size, in astrophysics comes mostly from Jeong et al. (2000 & 2003) who investigated $(TiO_2)_N$ nucleation in pulsating AGB

Article published by EDP Sciences, to be cited as http://dx.doi.org/10.1051/0004-6361/201424621

stars. They computed the most probable cluster geometries for N = 1 ... 6 and recommend a surface tension value of σ_∞ = 618 erg cm^{-2}. Since then, more stable $(TiO_2)_N$ cluster geometries up to $N = 10$ have been published (e.g Calatayud et al. 2008, Syzgantseva et al. 2011). Efforts to link these small-scale nano regime properties to the large-scale micron-sized bulk properties and vice versa has been undertaken by Bromley et al. (2009) which noted problems in acquiring stable TiO_2 nanocluster geometries. In the present paper, we use these cluster geometries from the chemistry literature and compute Gibbs formation energies for these clusters using the GAUSSIAN package (Frisch et al. 2009; Sects. 2.2, 2.3) and then update the surface tension value. After demonstrating the relative abundances of the individual clusters (Sect. 3), we assess the results for seed formation rates resulting from the classical nucleation theory and from directly applying the cluster data (Sect. 4). We note that the need for calculating a seed formation rate arises from our kinetic treatment of cloud particle formation. Other authors chose to treat the cloud particles as in phase-equilibrium. For a comparison of these approaches, please refer to Helling et al. (2008). Section 4.2 compares the TiO_2 seed formation rates with SiO nucleation for which updated vapour pressure data is available. Section 5 demonstrates the influence of the nucleation data on the details of the cloud structure. We show that the question regarding the most suitable nucleation species cannot be answered without taking into account the surface growth (or evaporation) processes as they reduce (or enrich) the gas reservoir from which the seed particles form.

2. Modelling seed formation as the first step of astrophysical dust and cloud formation

Cloud formation in brown dwarfs and planets as well as dust formation in AGB stars and supernovae require knowledge of how the individual (cloud) particles/grains form. The very first process is the formation of condensation seeds, unless seeds are injected into a condensible gas like that present on Earth or into the ISM through supernovae and AGB star winds. Only the presence of condensation seeds allows the growth to massive (μm-sized) particles (dust grains or cloud particles). Recent developments in computational chemistry and progress in laboratory astrophysics allow for the assessment of the seed formation modelling as in Helling & Woitke who apply the modified classical nucleation theory to model the homogeneous nucleation of TiO_2 condensation seeds. Based on updated dust data, we further assess the impact of the nucleation treatment on the results of our cloud formation model in Sect. 5.

2.1. Nucleation theory

We only summarise essential steps and definitions needed for this paper. We refer the reader to Helling & Fomins (2013) and Gail & Sedlmayr (2014) for further background reading.

2.1.1. Classical nucleation theory

The stationary rate for a homogeneous, homomolecular nucleation process is given by

$$J_*^c(t) = \frac{\overset{\circ}{f}(N_*)}{\tau_{gr}(r_i, N_*, t)} Z(N_*) S(T) \cdot \exp\{(N_* - 1)\ln S(T)\} \quad (1)$$

with N_* the critical cluster size (see Eq. 12). The equilibrium cluster size distribution, $\overset{\circ}{f}(N)$ [cm^{-3}], can be considered a Boltzmann-like distribution in local thermal equilibrium,

$$\overset{\circ}{f}(N) = \overset{\circ}{f}(1) \exp\left(-\frac{\Delta G(N)}{RT}\right), \quad (2)$$

where $\overset{\circ}{f}(1)$ [cm^{-3}] is the equilibrium number density of the monomer (smallest cluster unit like TiO_2 or SiO) and $\Delta G(N)$ [kJ mol^{-1}] the Gibbs free energy change due to the formation of a cluster of size N from the saturated vapour at temperature T. The rate of growth for each individual cluster of size N is

$$\tau_{\rm gr}^{-1}(r_{\rm i}, N, t) = A(N)\alpha(r_{\rm i}, N) v_{\rm rel}(n_{\rm f}(r_{\rm i}), N) n_{\rm f}(r_{\rm i}, t), \quad (3)$$

where $A(N) = 4\pi a_0^2 N^{2/3}$ [cm^2] is the reaction surface area of an N-sized cluster, N is the number of monomers in a cluster, a_0 the hypothetical monomer radius, α is the efficiency of the reaction (assumed to be 1), $v_{\rm rel}$ [cm^{2}s^{-1}] is the relative velocity between a monomer and the cluster and $n_{\rm f}$ [cm^{-3}] the particle density of the molecule for the growth (forward) reaction ($\equiv \overset{\circ}{f}(1)$). The relative velocity is approximated by the thermal velocity (see Eq. 15 in Helling et al. 2001)

$$v_{\rm rel} = \sqrt{\frac{kT}{2\pi\bar{\mu}}} \approx \sqrt{\frac{kT}{2\pi m_{\rm x}}} \quad (4)$$

with $\bar{\mu} = 1/(1/m_x - 1/m_V)$, where m_x is the mass of the monomer molecule (e.g. TiO_2) and m_V the mass of a grain with volume V. For macroscopic grains, $m_V >> m_x$, hence $\bar{\mu} \approx m_{\rm x}$. Equation 1 also contains the supersaturation ratio S_N of a cluster with N monomers $S_N = \overset{\circ}{p}(N)/\overset{\circ}{p}_{sat}$ with the saturation vapour pressure

$$\frac{\overset{\circ}{p}_{sat}}{p^\ominus} = \exp\left(\frac{\Delta_{\rm f}^\ominus G_1(s) - \Delta_{\rm f}^\ominus G(1)}{RT_d}\right); \quad (5)$$

ΔG(N) can be expressed by a relationship to the standard molar Gibbs free energies in reference state "$\ominus$" (measured at a standard gas pressure and gas temperature) of formation for cluster size N

$$\Delta G(N) = \Delta_{\rm f}^\ominus G(N) + RT \ln\left(\frac{\overset{\circ}{p}_{sat}(T)}{p^\ominus}\right) - N\Delta_{\rm f}^\ominus G_1(s). \quad (6)$$

Combining Eqs. 5 and 6 results in

$$\Delta G(N) = \Delta_{\rm f}^\ominus G(N) - \Delta_{\rm f}^\ominus G(1) - (N-1)\Delta_{\rm f}^\ominus G_1(s), \quad (7)$$

where the right-hand side contains standard state values only ($\Delta_{\rm f}^\ominus G$(N) - standard Gibbs free energy of formation of cluster size N, $\Delta_{\rm f}^\ominus G(1)$ - standard Gibbs free energy of the monomer, $\Delta_{\rm f}^\ominus G_1$(s) - standard Gibbs free energy of formation of the solid

phase) which can be found by experiment or computational chemistry. We use the JANAF thermochemical table (Chase et al. 1985) where the standard states are given at $T^{\circ}_{\rm gas} = 298.15$K and $p^{\circ}_{\rm gas} = 1$ bar.

The classical nucleation theory assumes that the detailed knowledge about ΔG(N) can be encapsulated by the value of the surface tension, σ_∞, of the macroscopic solid such that

$$\frac{\Delta G(N)}{RT} = -N\ln(S) + \theta_\infty N^{2/3} \quad \text{with} \quad \theta_\infty = \frac{4\pi a_0^2 \sigma_\infty}{k_b T}. \tag{8}$$

The dependence of the surface energy on cluster size is therefore neglected. The Zeldovich factor (contribution from Brownian motion to nucleation rate) in Eq. 1 is

$$Z(N_*) = \left(\frac{\theta_\infty}{9\pi(N_*-1)^{4/3}} \frac{(1+2(\frac{N_f}{N_*-1})^{1/3})}{(1+(\frac{N_f}{N_*-1})^{1/3})^3} \right)^{1/2}. \tag{9}$$

The nucleation rate can now be expressed as

$$J^c_*(t) = \frac{\overset{\circ}{f}(1,t)}{\tau_{gr}(1,N_*,t)} Z(N_*) \exp\left((N_*-1)\ln S(T) - \frac{\Delta G(N_*)}{RT} \right). \tag{10}$$

2.1.2. Modified classical nucleation theory

A modified nucleation theory was proposed by Draine et al. (1977) and Gail et al. (1984) by taking into account the curvature on the surface energy for small clusters (Gail et al. 1984). Equation 8 changes to

$$\frac{\Delta G(N)}{RT} = \theta_\infty \frac{N-1}{(N-1)^{1/3} + N_f^{1/3}}, \tag{11}$$

where N_f is a fitting factor representing the particle size at which the surface energy is reduced to half of the bulk value. This fitting factor allows a critical cluster N_* to be calculated as

$$N_* - 1 = \frac{N_{*,\infty}}{8} \left(1 + \sqrt{1 + 2\left(\frac{N_f}{N_{*,\infty}}\right)^{1/3}} - 1 \left(\frac{N_f}{N_{*,\infty}}\right)^{1/3} \right)^3 \tag{12}$$

with

$$N_{*,\infty} = \left(\frac{\frac{2}{3}\theta_\infty}{\ln S(T)} \right)^3. \tag{13}$$

2.1.3. Non-classical nucleation theory

If cluster data are available, J_* can be calculated using cluster number densities, growth rates and evaporation rates of each cluster size as J_* is a flux through cluster space,

$$J_*(N) = \frac{\overset{\circ}{f}(N-1)}{\tau_{gr}(N-1)} - \frac{\overset{\circ}{f}(N)}{\tau_{ev}(N)}. \tag{14}$$

Applying the Becker-Döring method (see Gail & Sedlmayr 2014), $f(2)$ can be eliminated from the $N = 2$ equation using the $N = 3$ equation, then again for $f(3)$ and so on, resulting in the summation

$$J_*^{-1}(t) = \sum_{N=1}^{N_{max}} \left(\frac{\tau_{gr}(r_i, N, t)}{\overset{\circ}{f}(N)} \right) \tag{15}$$

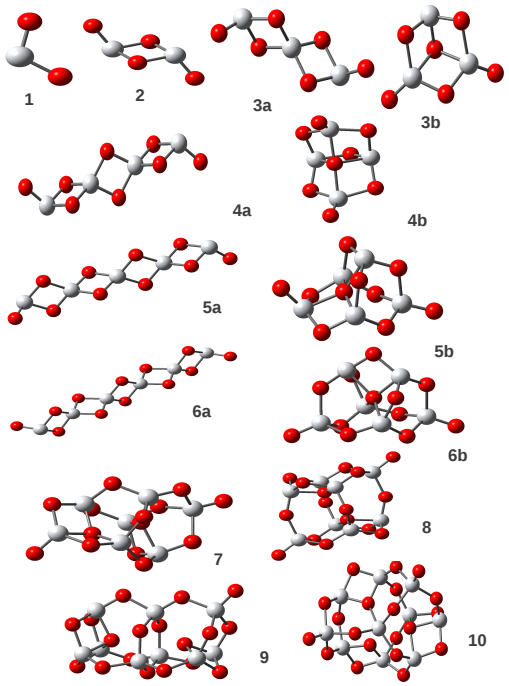

Fig. 1. Geometry of the calculated $(TiO_2)_N$ structures. Molecules labelled "a" are the molecules calculated by Jeong et al. (2000) and those labelled "b" or unlabelled are the current most stable cluster geometries (Calatayud et al. 2008, Syzgantseva et al. 2011). Grey balls represent Ti atoms while red represent O atoms.

with Eq. 3 for τ_{gr}. The number density of a cluster of size N is

$$\overset{\circ}{f}(N) = \frac{\overset{\circ}{p}(N)}{kT}. \tag{16}$$

The partial pressures can be calculated from the law of mass action applied to an N-cluster,

$$\overset{\circ}{p}(N) = p^{\circ} \left(\frac{\overset{\circ}{p}(1)}{p^{\circ}} \right)^N \exp\left(-\frac{\Delta^{\circ}_f G(N) - N\Delta^{\circ}_f G(1)}{RT} \right), \tag{17}$$

with $\overset{\circ}{p}(1)$ [dyn cm^{-2}] the partial pressure of the monomer number density; $\overset{\circ}{p}(1)$ will be calculated as local thermodynamic equilibrium (LTE) allowing the application of our equilibrium chemistry routine (Sect. 3.1.2).

2.2. Approach

2.2.1. Computational aspects

All cluster calculations were performed using the B3LYP (Lee et al.1988) density functional theory with basis set 6-311G(d) as part of the Gaussian (Frisch et al. 2009) computational chemistry package. This level of theory was used for its mix of accuracy and computational speed and to keep in line the previous investigations on the same molecules (Jeong et al. 2000, Calatayud et al. 2008, Syzgantseva et al. 2011). B3LYP is a popular and well regarded density functional theory for

metal oxides and other inorganic compounds. The reference state of the clusters was at temperature $T^{\ominus}$ = 298.15K and pressure $p^{\ominus}$ =1 bar. These were chosen so that the JANAF thermochemical tables for the elemental thermochemical values could be used to calculate the Gibbs free energies of the molecules. Gaussian calculates the partition function of a molecule using thermodynamical laws with contributions from the rotational, translational, vibrational and electronic motions of the molecule. Therefore, it can generate enthalpies (ΔH) and Gibbs energies (ΔG) for any molecule to a good degree of accuracy depending only on the functional and basis set used. These enthalpies and Gibbs free energies can then be used to find the formation energies of the molecules with basic thermodynamics (Sect. 2.3). Previous studies of these TiO_2 cluster geometries (Calatayud et al. 2008, Syzgantseva et al. 2011) have focused on the reactivity and electronic structure of the clusters and not specifically on the thermodynamics of the formation of the clusters themselves.

2.2.2. Cluster geometries

The main difference between past investigations and the current study are the calculation of updated TiO_2 cluster geometries. Figure 1 summarises both the original geometries from Jeong et al. (2000) labelled "a", with the new results labelled "b" or unlabelled. These geometries can mostly be found in the chemistry literature (Calatayud et al. 2008, Syzgantseva et al. 2011, Richard et al. 2010) except for a new stable N=7.

The linear, polymer-like $(TiO_2)_N$ chains investigated in Jeong et al. (2000) are less stable than their more compressed counterparts published by Calatayud et al. 2008 and Syzgantseva et al. 2011. This is shown by the higher binding energies for the compressed structures (Appendix A). These binding energies have a direct impact on the Gibbs formation energies of the clusters and there will be significant differences between the two geometries. Furthermore, it is assumed that over time the molecules will configure to their lowest energy state geometry and so other less stable configurations are not considered further.

2.3. Results for thermodynamic quantities for TiO_2 clusters

Applying the results of the computation to thermodynamical identities allows the calculation of the Gibbs free energies of the clusters. The Gibbs energy of formation can be calculated from

$$\Delta_{\rm f}G^{\circ}(M,T) = \Delta_{\rm f}H^{\circ}(M,T) - T\left(S^{\circ}(M,T) - \sum_{\rm elements} xS^{\circ}(X,T)\right), \quad (18)$$

where M is the molecular/cluster values and X the constituent atoms. In order to find the enthalpy of formation of a cluster at temperature T the enthalpy of formation at 0K must first be calculated. This is given by

$$\Delta_f H^{\circ}(M,0K) = \sum_{atoms} x\Delta_f H^{\circ}(X,0K) - \sum D_0(M), \quad (19)$$

where x is the total number of elements X in the molecule and $D_0(M)$ the reduced atomization energy of the molecule. The $\Delta_f H^{\circ}(X,0K)$ of Ti and O can be found in the JANAF thermochemical tables. The reduced atomization energy in Eq. **??** is defined as

$$\sum D_0(M) = \left(\sum_{elements} xE_0(X) - E_0(M) - E_{zpe}(M)\right), \quad (20)$$

where $E_0(X)$ and $E_0(M)$ are the internal energy of the elements and the molecule and $E_{zpe}(M)$ the zero-point energy of the molecule. All the total energy terms ($E_0(X)$, $E_0(M)$, and $E_{zpe}(M)$) can be calculated from the Gaussian 09 output. The crucial quantity of the elemental atomization energies($E_0(X)$) of both Ti and O was computed using the same level of theory (B3LYP 6-311G(d)) as the clusters.

When the enthalpy of formation at 0K is calculated for each cluster, we can find the enthalpy of formation at a reference temperature ($T^{\ominus}$ = 298.15K) as

$$\Delta_f H^{\circ}(M,298K) = \Delta_f H^{\circ}(M,0K) + (H^{\circ}_M(298K) - H^{\circ}_M(0K)) - \sum_{elements} x(H^{\circ}_X(298K) - H^{\circ}_X(0K)). \quad (21)$$

The enthalpy of formation at arbitrary temperature T can then be found by a similar calculation:

$$\Delta_f H^{\circ}(M,T) = \Delta_f H^{\circ}(M,298K) + (H^{\circ}_M(T) - H^{\circ}_M(298K)) - \sum_{elements} x(H^{\circ}_X(T) - H^{\circ}_X(298K)). \quad (22)$$

The entropy of the clusters are calculated from the relation $S = (H-G)/T$ where H and G are the enthalpy and Gibbs energies, respectively. The entropy of the constituent elements at various temperatures are from the JANAF thermochemical tables.

Calculated thermochemical tables and Gibbs free energies for the $(TiO_2)_N$ clusters are provided in Appendix B.

2.3.1. Surface tension of TiO_2

Surface tension is a measure of surface energy density of the bulk property of a solid. We approximate the bulk surface tension, σ_∞, by fitting the small clusters to the modified nucleation theory using the calculated Gibbs free energies. Combining Eqs. 6 and 11, the Gibbs formation energy of cluster size N is

$$\frac{\Delta_f G(N)}{N} = \theta_\infty RT\frac{N-1}{(N-1)^{1/3}+N_f^{1/3}} + \Delta_f^{\ominus}G(1) + (N-1)\Delta_f^{\ominus}G_1(s). \quad (23)$$

By plotting $\Delta G_f(N)/N$ against N for the clusters, a best fit σ_∞ can be found for different temperatures. Figure 2 shows this fitting process for T = 1000 K. The original surface tension value from Jeong et al. (2000), σ_∞ = 618 erg cm^{-2}, is also shown for comparison. The values for $\Delta_f^{\ominus}G_1(s)$ are from the JANAF tables and N_f = 0 is used for all calculations. The new cluster geometries have a lower Gibbs energy of formation than the old clusters as a consequence of their increased stability. By fitting σ_∞ we show that there is a slight temperature dependence

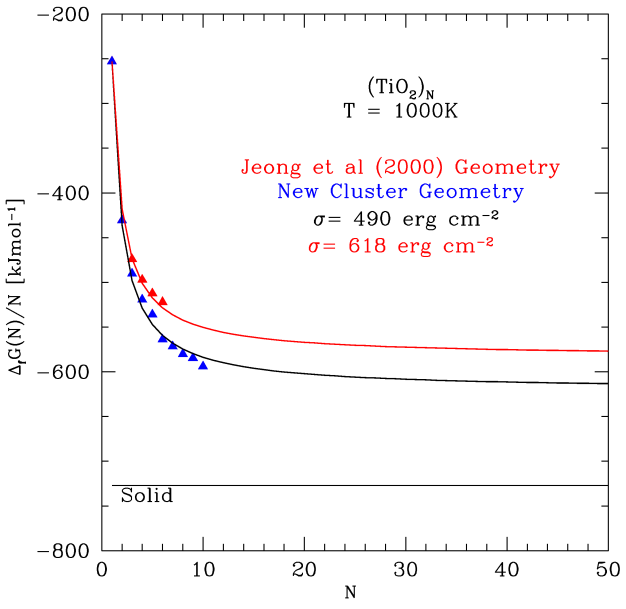

Fig. 2. TiO_2 Δ_f G(N)/ N with respect to N for T = 1000K. The blue triangles represent the new geometry isomers while red represent the molecules found in Jeong et al. (2003). The red line is the modified expression with σ_∞ = 618 erg cm^{-2} and the black with σ_∞ = 490 erg cm^{-2}.

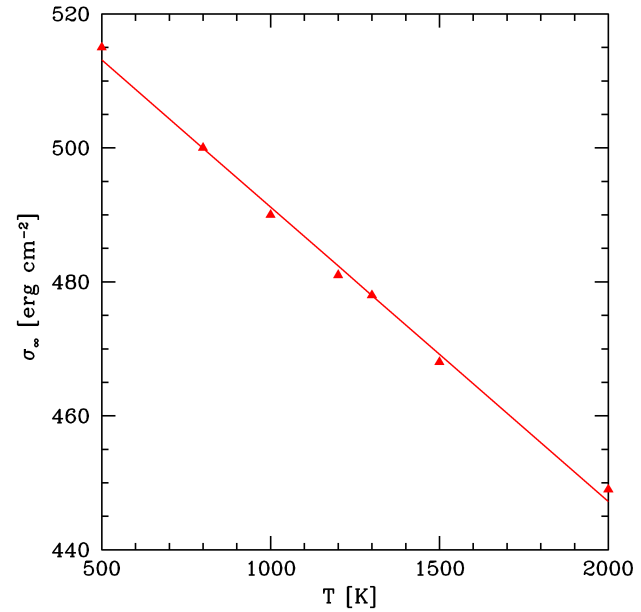

Fig. 3. Temperature dependence of best fit σ_∞ for the range T_{gas} = 500 - 2000 K. Triangles denote best fit values to the modified nucleation expression.

(Fig. 3) on the best fit value. In the range T_{gas} = 500 - 2000K the surface tension can be approximated by the linear relationship

$$\sigma_\infty(T_{gas}) = 535.124 - 0.04396 T_{gas}. \quad (24)$$

The mean value over this temperature range yields an approximate surface tension of σ_∞ = 480.6 erg cm^{-2}.

3. The abundances of molecules and clusters in the gas phase

The seed formation rates depend on the gas-phase composition and the abundance of the monomer gas-species in comparison. We therefore summarise the abundances of the Ti-binding gas-species and we include Si-binding molecules for later considerations of SiO nucleation based on updated SiO vapour pressure data. We apply our thermodynamic cluster data to explore the abundance of the TiO_2 clusters shown in Fig. 1 and their relative changes.

3.1. Approach

We utilize one example model atmosphere structure (T_{eff} = 1600K, log(g)=3.0, solar metallicity) from the Drift-Phoenix atmosphere grid that is representative for the atmosphere of a giant gas planet and for brown dwarfs. This combination of global parameters also includes the atmosphere of the group of recently discovered low-gravity brown dwarfs (Faherty et al. 2013). We use the model (T_{gas}, p_{gas}) structure as input for our external chemical equilibrium program to calculate the chemical gas composition in more detail than necessary for the Drift-Phoenix models.

3.1.1. Drift-Phoenix model atmosphere

Drift-Phoenix (Dehn 2007, Helling et al. 2008b, Witte et al. 2009) model atmosphere simulations solve the classical 1D model atmosphere problem coupled to a kinetic phase-non-equilibrium cloud formation model. Each of the model atmospheres is determined by the effective temperature (T_{eff} [K]), the surface gravity (log(g) (with g in cm/s^2) and element abundances. The cloud's opacity is calculated applying Mie and effective medium theory.

In addition to details of the dust clouds like height-dependent grain sizes and the height-dependent composition of the mixed-material cloud particles, the atmosphere model provides us with atmospheric properties such as the local convective velocity, the temperature-pressure (T_{gas} [K], p_{gas} [dyn/cm^2]) structure and the dust-depleted element abundances. The local temperature is the result of the radiative transfer solution, the local gas pressure of the hydrostatic equilibrium and the element abundances are the result of the element conservation equations that include the change of elements by dust formation and evaporation.

3.1.2. Chemical equilibrium routine

A combination of 155 gas-phase molecules (including 33 complex carbon-bearing molecules), 16 atoms and various ionic species were used under the assumption of LTE. For more details, please refer to Bilger, Rimmer & Helling (2013) and Helling, Winters & Sedlmayr (2000) for the thermodynamical data used. The Grevesse, Asplund & Sauval (2007) solar composition is used to calculate the gas-phase chemistry outside the metal depleted cloud layers and before cloud formation. No solid particles were included in the chemical equilibrium cal-

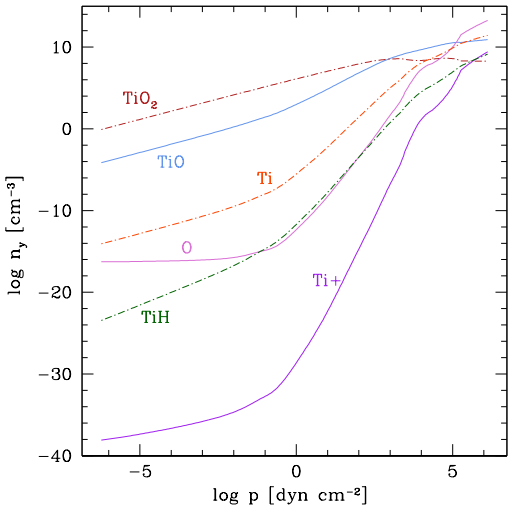

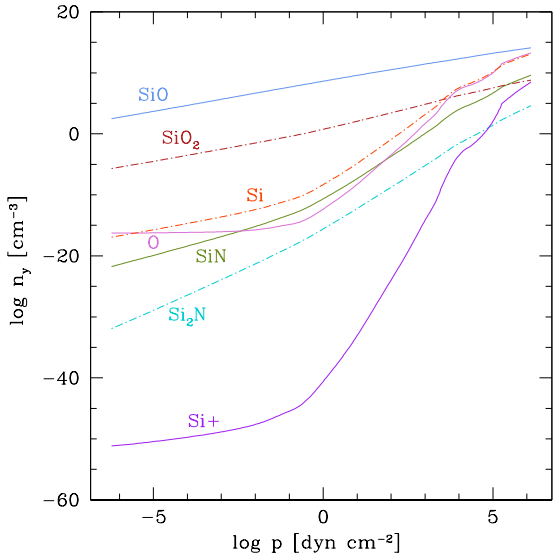

Fig. 4. Comparison of number densities (cm^{-3}) for different Ti-binding (top) and Si-binding (bottom) molecules for a DRIFT-PHOENIX (T_{gas}, p_{gas}) structure for T_{eff}=1600K, log(g)=3.0 and solar metallicity.

culations. However, their presence influences the gas phase by reducing element abundances from cloud formation and the impact of the cloud opacity on the radiation field, both accounted for in the DRIFT-PHOENIX model simulations. We utilize DRIFT-

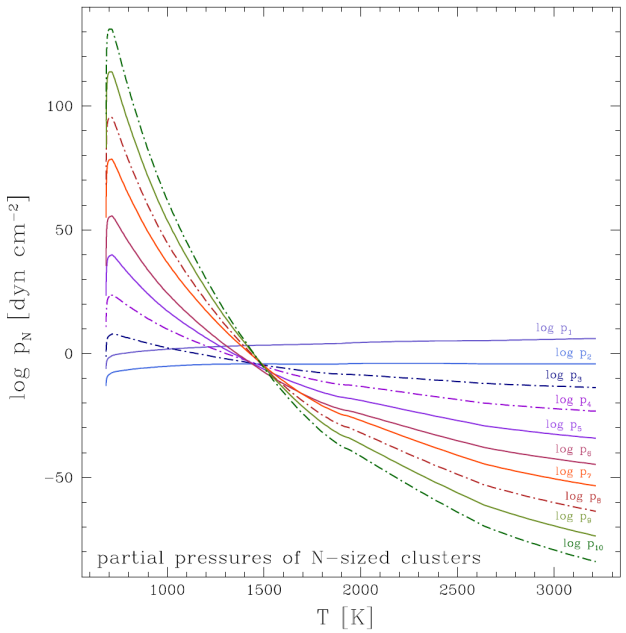

Fig. 5. Partial pressures $\mathring{p}$(N) for N=1,10 (dyn cm^{-2}) in chemical equilibrium. Each calculation uses the standardized pressure p° and the Gibbs free energies from Sect. 2.3.

PHOENIX model atmosphere (T_{gas}, p_{gas}) structures as input for our calculations.

3.2. Results for molecule and cluster abundances

As pressure and temperature increase in the atmosphere, the abundance of all gas species increase in chemical equilibrium (Fig. 4). For comparison, both Ti and Si combinations are shown because the number densities of TiO_2 and SiO are input properties for Eqs. 10 and 17. The SiO molecule generally has a higher number density than TiO_2 since the element abundance of Si is considerably larger than that of Ti. This might suggest that SiO is a more suitable nucleation species than TiO_2 and we will investigate this question in Sects. 4.2 and 5. Figure 4 (top) demonstrates that TiO_2 is the most abundant Ti-binding gas species in almost the entire atmosphere followed by TiO and the Ti atom. The molecule TiO is more abundant than TiO_2 in the high-temperature part of the atmospheric structure; SiO is the most abundant Si-binding molecules followed by SiO_2 and Si.

As part of our assessment of the TiO_2 nucleation, we show the partial pressure, $\mathring{p}$ (N) [dyn cm^{-2}] (Eq. 17), for each $(TiO_2)_N$ cluster in Fig. 5. Both $\mathring{p}(1)$ (= $n_{TiO_2} kT_{gas}$) and $\mathring{p}(2)$ maintain fairly constant pressures. For $N > 2$, the curves become more dynamic. They start at higher and higher magnitudes, increase quickly, and then drop off. The order of the curves is also interesting, with the higher N partial pressures reaching higher values at lower temperature (lower gas pressures). These findings support our expectation that bigger clusters become more stable and more abundant with decreasing temperatures and that they are unstable and of low abundance at high temperatures.

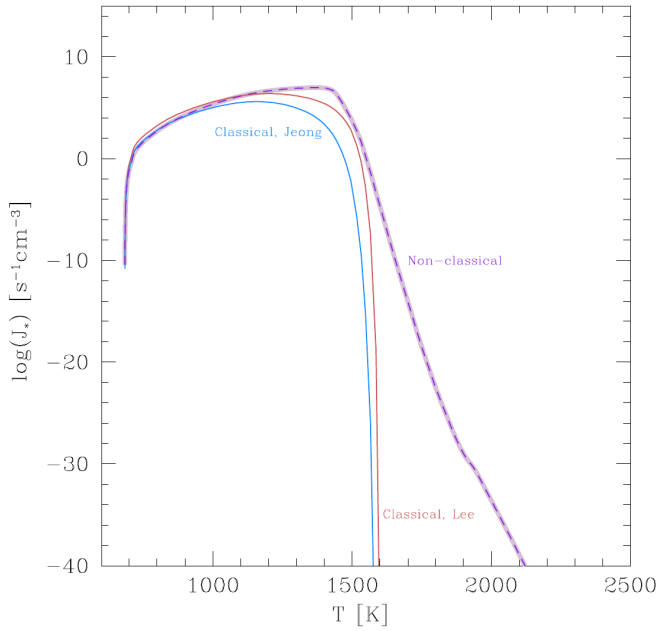

Fig. 6. Nucleation rates J_* with three methods: classical with $\sigma_\infty = 618$ erg cm^{-2}, Jeong et al. (2000); classical with temperature dependent σ_∞; and non-classical based on Gibbs free energies for TiO_2.

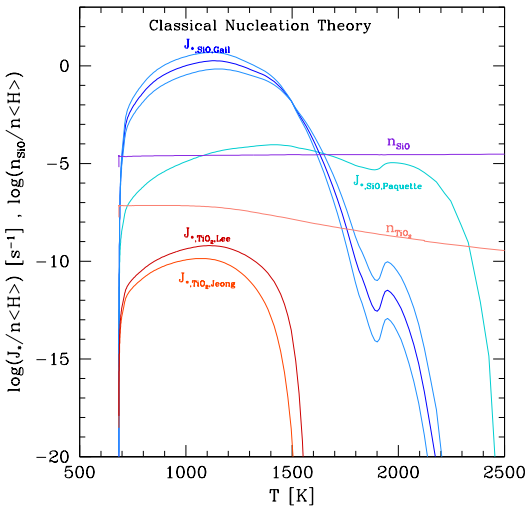

Fig. 7. Number densities (cm^{-3}) and nucleation rates J_* (s^{-1}cm^{-3}) for both TiO_2 and SiO. Number densities calculated from the DRIFT-PHOENIX model (Ch. Helling et al. 2006). $J_{*,\mathrm{Jeong}}$ is the classical nucleation rate calculated with $\sigma_\infty = 618$ erg cm^2; $J_{*,\mathrm{Lee}}$ is calculated with temperature dependent σ_∞. $J_{*,\mathrm{Paquette}}$ and $J_{*,\mathrm{Gail}}$ have both been calculated using new vapour pressures (Wetzel et al. 2012). Blue lines surrounding $J_{*,\mathrm{Gail}}$ are the upper and lower boundaries. These nucleation rates were calculated for an undepleted gas-phase.

4. Seed formation rates

Based on the results from Sects. 2.3.1 and 2.3.2, we are now in the position to calculate and compare seed formation rates (nucleation rates). We present our updated results for TiO_2 as the nucleation species considered in our previous works. We compare SiO nucleation based on updated vapour pressure data. Gail et al. (2013) has recently suggested that SiO nucleation could be more efficient than TiO_2 nucleation. We will test this hypothesis here and as part of our cloud formation model in Sect. 5.

4.1. TiO_2 nucleation rate

Results for classical nucleation theory: Surface tension values have a direct impact on the nucleation rate in the classical nucleation theory approach (Sect. 2.1.1). In order to assess this impact, the new TiO_2 surface tension was tested in our nucleation routines and nucleation rates calculated for a given (T_{gas}, p_{gas}) model atmosphere profile. Figure 6 demonstrates that the difference in nucleation rate, J_*, from our new data to the value from Jeong et al. (2000) is not very significant.

Results for non-classical nucleation theory: Converting all partial pressures, $\mathring{p}$ (N), for all $(TiO_2)_N$ cluster into number densities allows us to use the Becker-Döring method to calculate the nucleation rate J_* (Gail & Seldmayr 2014). This is different from the classical nucleation rate in that we use the Gibbs free energies of formation for each individual cluster without the need to derive a surface tension.

Figure 6 shows that at the lowest temperatures, the non-classical nucleation rate increases quickly with the temperature until 700K where the rate increases more slowly to around 1800K, and then drops (though not as quickly as the classical curves). At the higher temperatures, the molecules will have sufficient energy so that when they collide they will break apart just as often as they coalesce. Though the non-classical values are visibly different from the classical, they are similar in magnitude to the classical data with a temperature varying σ_∞, particularly in the 700-1500K region of the model atmosphere considered here.

4.2. SiO nucleation

Stimulated by the recent paper by Gail et al. (2013), we compare the nucleation rate of SiO to our TiO_2 values from the previous sections. Since the number density of SiO is much greater than TiO_2, it is reasonable to expect that the nucleation rate for SiO would also be larger than that of TiO_2. Gail et al. (2013) provide the following analytic expression for the SiO nucleation rate including the updated vapour pressure from Wetzel et al. (2012),

$$J_*^{\mathrm{SiO}} = n_1^2 \exp\left((1.33 \pm 3.1) - \frac{(4.40 \pm 0.61) \cdot 10^{12}}{T^3 (\ln S)^2}\right), \qquad (25)$$

where $n_1 = \mathring{f}(1)$ and all other variables have the same meaning as before. Calculating J_*^{SiO} for the same model atmosphere structure as before, we find that SiO nucleates at a much higher rate compared to our TiO_2 results. We also demonstrate in Fig. 7 the changes in the SiO nucleation rates alone through the update in vapour pressure data, $J_{*,\mathrm{Paguette}}$ vs. $J_{*,\mathrm{Gail}}$. There are similarities between the two SiO rates, the double peaks occur at approximately the same temperatures, indicating that

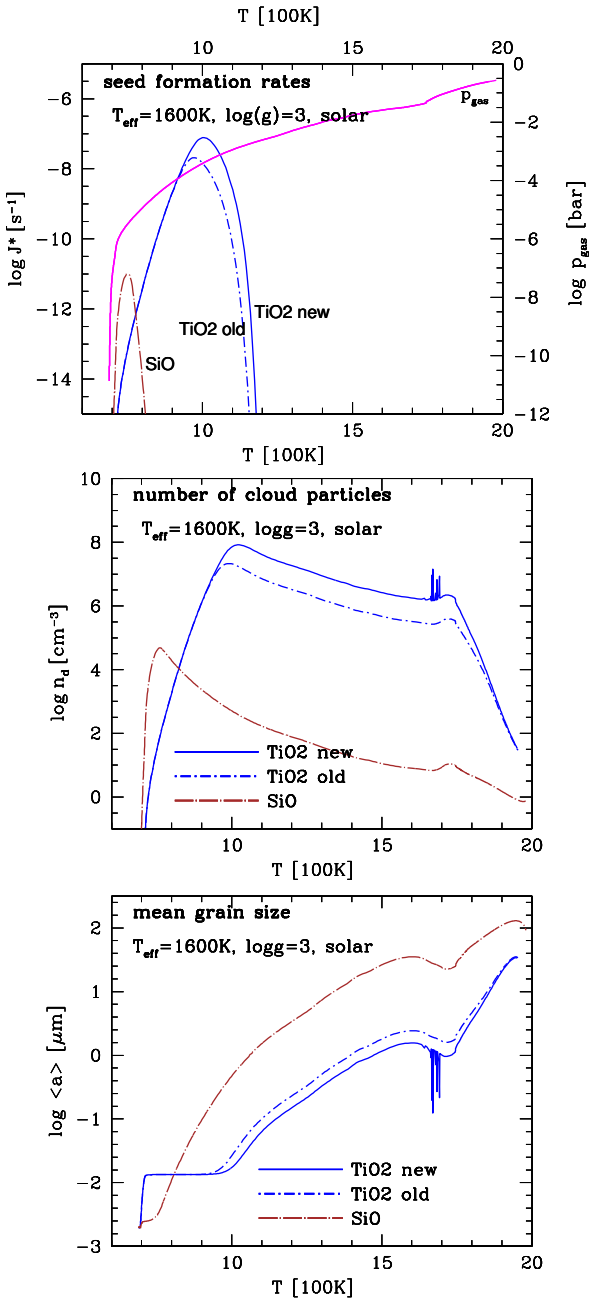

Fig. 8. TiO_2 and SiO nucleation rates (top) calculated as part of the cloud formation model and their effect on the number density of cloud particles (middle) and the mean grain size (bottom). The calculations include nucleation, growth/evaporation, element conservation, gravitational settling, and convective replenishment. The same DRIFT-PHOENIX model structure for T_{eff} = 1600K, log(g)=3.0, and solar metallicity as in Fig. 6 was used.

both methods create similar effects at these temperatures. These differences resulting from updated vapour pressure data cannot account for the differences between the SiO and the TiO_2 nucleation rates.

5. Impact on cloud formation

Cloud formation in brown dwarfs and giant gas planets needs to start with the formation of condensation seeds in contrast to the Earth where weather cloud formation is started through the injection of seed particles (e.g. volcano eruptions or sand storms) into the atmosphere. Jeong et al. (1999) demonstrate that it is not obvious which species would be the best choice for a nucleation species as part of a dust / cloud particle formation model. Gail et al. (2013) and Helling & Fomins (2013) further argue that the complex silicate seeds (e.g. Mg_2SiO_4[s], Al_2O_3[s]) can only form from molecules that are available in the gas-phase. The SiO and TiO_2 are available in abundance in the gas phase (Fig. 4), but Mg_2SiO_4 does not exist as a molecule, and Al_2O_3 is extremely rare (e.g. Fig. 5 in Helling & Woitke 2006). Other Mg or Al binding molecules are abundant pointing to the possibility of heterogeneous nucleation. Hence, the formation of seed particles does not need to proceed via a homomolecular homogeneous nucleation, but may well be formed by heteromolecular homogeneous nucleation (e.g. Goumans & Bromley 2013, Plane 2013). Because of the lack of cluster data for more complex nucleation paths, we consider homomolecular homogeneous nucleation only.

In principle, the condensing material does not care which seed particle is available as long as there is a surface to condense on. The need to identify the first condensate or the most efficient nucleation species arises if a model is built in order to study dust forming systems, for example, clouds in brown dwarfs and exoplanets, or dust in circumstellar shells. The two best candidates with respect to stability and abundance in the gas phase are TiO_2 and SiO. We are now in the position to test how the new material data for TiO_2 (Sect. 2.3) and the updated saturation vapour pressure for SiO (Eq. 25) affect our cloud formation results. Our results in this paper have so far lead us to expect only moderate differences from the updated TiO_2 nucleation rate (Fig. 6), but substantial differences if considering SiO instead of TiO_2 as the nucleation species. Figure 7 suggests a considerably more efficient SiO seed formation compared to TiO_2 seed formation. In this section, we will demonstrate that it is misleading to consider seed formation as a single process. The nucleation process needs to be considered in combination with other element consuming cloud/dust formation processes in order to reliably approach the question about the most suitable condensation seed species.

5.1. Approach

We assess the impact of the nucleation description that is part of our cloud formation model on the resulting cloud structure details. Our cloud formation model describes the formation of clouds by nucleation, subsequent growth by chemical surface reactions on-top of the seeds, evaporation, gravitational settling, element conservation, and convective replenishment (Woitke & Helling 2003, 2004; Helling & Woitke 2006, Helling et al. 2008a). The effect of nucleation, growth, and evaporation on the remaining elements in the gas phase is fully accounted for (Eqs. 10 in Helling, Woitke & Thi 2008a). The surface growth causes the grains to grow to μm-sized particles of a mixed composition of those solids taken into account. For this study, we consider 12 growth species that grow by 60 gas-solid surface reactions (Helling et al. 2008a). We use the same

Drift-Phoenix model atmosphere as described in Sect. 3.1 as input for our more complex cloud formation code.

5.2. Results

Figure 8 demonstrates the impact of the nucleation treatment on the cloud formation processes and the resulting cloud properties. Most importantly, if considered as part of an interacting set of processes, the TiO_2 seed formation is more efficient than the SiO seed formation (top panel with nucleation rates) which deviates from our previous expectation triggered by Fig. 7. The reason is that the elements Si and O are part of many silicate materials (SiO_2[s],$MgSiO_3$[s], Mg_2SiO_4[s], etc.) that are already thermally stable and therefore grow efficiently as soon as the seed particles emerge from the gas phase. Ti-binding growth species are much less abundant because of the low Ti element abundances to start with (Fig. 4). Hence, an assessment of the importance of a seed forming species always needs to be performed in connection with the growth process, else it leads to wrong conclusions regarding the best suited nucleation species. As a consequence of SiO being a very inefficient nucleation species, fewer cloud particles form. Figure 8 (middle) shows that a SiO-seeded cloud would have $> 10^3$ times fewer cloud particles with an increasing difference for increasing atmospheric depth. Instead, the material is consumed by growth leading to grains up to a size of 100μm at the inner cloud edge.

Figure 9 demonstrates that the overall mean material composition of the mineral cloud does not change significantly between TiO_2-seeded and SiO-seeded clouds. However, the uppermost part, which is often referred to as the haze layer, has a fundamentally different composition depending on the condensation seed species considered: SiO[s]/MgO[s] with impurities of FeS[s], FeO[s], Fe_2O_3[s], and Al_2O_3[s] in the case of SiO nucleation, and $MgSiO_3$[s]/Mg_2SiO_4[s] with impurities of all other solids plus a very thin TiO_2[s] layer at the very top in the case of TiO_2[s] nucleation.

6. Summary

The formation of condensation seeds is the initial step to cloud formation in astrophysical objects without a crust, for example supernovae, AGB-stars, M-dwarfs, brown dwarfs, and giant gas planets. The long-standing question is whether it is possible to identify a first condensate that kicks off the whole condensation process. This question has long been debated. High-temperature condensates such as solid iron seeds forming from $(Fe)_N$ gas phase clusters (John & Sedlmayr 1997) or MgO seeds forming from $(MgO)_N$ clusters (Köhler & Sedlmayr 1997) were dismissed because large clusters were thermodynamically unstable or they were not very abundant. Instead, TiO_2 seed formation is attractive because of the stability of the $(TiO_2)_N$ clusters and their relative abundance. The same arguments are made for SiO, but despite SiO's higher abundance compared to TiO_2, its nucleation rate did fall short of TiO_2 (Jeong et al. 2000). Gail et al. (2013) reconsider SiO nucleation for AGB stars and suggest that it might be a favourable seed formation species based on new vapour data. Based on updated $(TiO_2)_N$ clusters we investigate under which conditions this finding could be relevant for substellar atmospheres.

In this paper, we have presented updated Gibbs free energies of TiO_2 clusters using computational chemistry for newly available molecule geometries (Calatayud et al. 2008, Syzgantseva et al. 2011). The more stable cluster geometries compared to Jeong et al. (2000) from chemistry literature yielded a temperature dependent surface tension with an average value of $\sigma_\infty = 480.6$ erg cm^{-2} when fitted with the modified nucleation theory model. This new surface tension was then used in conjunction with chemical abundance routines to calculate a nucleation rate for various temperatures and TiO_2 number densities for an example atmosphere representative of a young brown dwarf or a giant gas planet. The new value approximately doubles the rate of nucleation for the species. The non-classical TiO_2 nucleation rate was calculated using the newly calculated Gibbs free energies which obtained higher results than those obtained through classical means. Inspired by newly available vapour pressure data, we show that SiO nucleation can only be more efficient than TiO_2 nucleation if no other element depletion processes are taking place. Hence, TiO_2 remains the more efficient nucleation species of the two because nucleation and surface growth will take place simultaneously and because both processes require a supersaturated gas.

Acknowledgements. We highlight financial support of the European Community under the FP7 by an ERC starting grant. We are very grateful for a scholarship fund for GL and HG by the Royal Astronomical Society. We thank Peter Woitke for general discussions on the paper's topic. The computer support at the School of Physics & Astronomy in St Andrews is gratefully acknowledged.

References

Bilger C., Rimmer P.B., Helling Ch. 2013, MNRAS 435, 1888
Bromley S.T., Moreira I.P.R., Neyman K.M., and Illas F 2009, Chem. Soc. Rev, 38, 2657-2670
Calatayud M., Maldonado L., and Minot C 2008, J.Phys. Chem. C, 112, 16087-16095
Catlow C. R. A., Bromley S. T., Hamad S., Mora-Fonz M., Sokol A. A., Woodley S. M. 2010, Phys. Chem. Chem. Phys. 12(4), 786
Chase M.W, Davies C.A, Downey J.R, Frurip D.J, McDonald R.A, and Syverud A.N 1985, NIST-JANAF thermochemical tables 1985
Copperwheat C.M., Wheatley P.J., Southworth J., Bento J., Marsh T.R. et al. 2013, MNRAS 434, 661
Demyk K., Heijnsbergen D., Helden G., and Meijer G. 2004, A&A 420, 547-552
Dehn M., 2007, PhD thesis, Univ. Hamburg
Faherty J., Rice E., Cruz K.L., Mamajek E.E., Nunez A. 2013, AJ 145, 2
Frisch M.J., Trucks G.W., Schlegel H. B., Scuseria G. E., Robb M. A. et al. 2009, Gaussian 09 Revision D.01, Gaussian Inc. Wallingford CT 2009
Gail H.P., Keller R Sedlmayr E. 1984, A&A 133, 320
Gail H.P., Sedlmayr E. 1986, A&A 166, 225
Gail H.P., Wetzel S., Pucci A., Tamanai A. 2013, A&A 555, 119

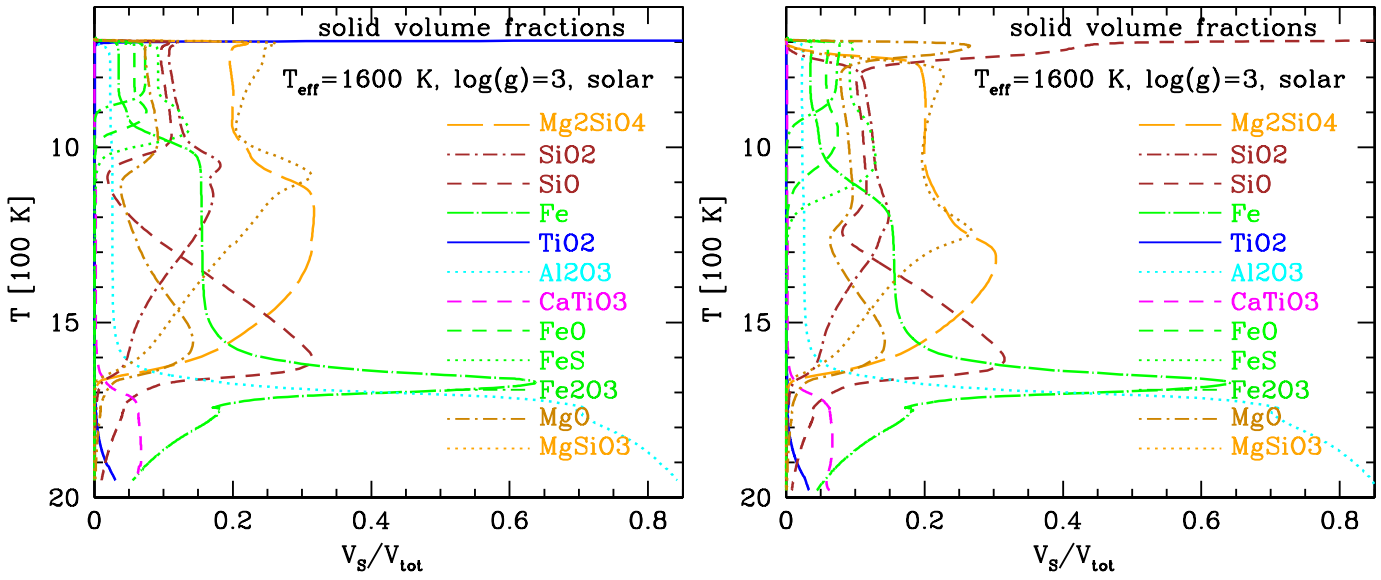

Fig. 9. The differences in the cloud particle material compositions for TiO_2 nucleation (left) and SiO (right). The nucleation species (TiO_2 or SiO molecule) are also surface growth species (as in Table 1 in Helling, Woitke & Thi 2008). The main differences occur in the uppermost part of the cloud, the haze layer: SiO[s]/MgO[s] with impurities of FeS[s], FeO[s], Fe_2O_3[s], and Al_2O_3[s] in the case of SiO nucleation (right), and $MgSiO_3$[s]/Mg_2SiO_4[s] with impurities of all other solids plus a very thin TiO_2[s] layer at the very top in the case of TiO_2[s] nucleation (left).

Gail H.P., Sedlmayr E. 2014, Physics and Chemistry of Circumstellar Dust Shells, Cambridge Astrophysics Series 52
Grevesse N., Asplund M., Sauval A. J., 2007, Space Sci. Rev.,130, 105
Goumans T.P.M., Bromley S.T. 2013, Phil. Trans. R. Soc. A 371 (1994), 20110580
Helling Ch., Winters J.-M., Sedlmayr E. 2000, A&A 358, 651
Helling Ch., Oevermann M., Lüttke M.J.H., Klein R., Sedlmayr E. 2001, A&A 376, 194
Helling Ch., Woitke P. 2006, A&A 455, 325
Helling Ch. 2007, Proceedings of the International Astronomical Union (2006) 2, 224
Helling Ch., Woitke P., Thi W.-F. 2008a, A&A 485, 547
Helling Ch., Dehn M., Woitke P., Hauschildt P. H. 2008b, ApJ 675, L105
Helling Ch., Ackerman A., Allard F., Dehn M., Hauschildt P., Homeier, D. et al. 2008, MNRAS 391, 1854
Helling Ch., Fomins A. 2013, Phil. Trans. R. Soc. A 37 (1994), 20110581-20110581
Jeong K.S., Winters J.M., Sedlmayr E. Proceedings of the International Astronomical Union (1999), 99-62044, 233
Jeong K. S., Chang C., Sedlmayr E., Sülzle D. 2000, JPhB 33, 3417
Jeong K. S, Winters J. M., Le Bertre T., Sedlmayr E. 2003, A&A 407, 191
John M., Sedlmayr E. 1997, ApSS 251, 219
Köhler T.M., Sedlmayr E. 1997, A&A 310, 553
Lecavelier Des Etangs A., Pont F., Vidal-Madjar A., Sing D. 2008, A&A 481, 83
Lee C., Yang W., Parr R. G. 1988, Phys. Rev. B37, 785
Miller-Ricci Kempton E., Zahnle K., Fortney J.J. 2012, APJ 745, 3
Patzer A.B.C, Gauger A., and Sedlmayr E. 1998, A&A 337, 847-858
Richard C., Catlow A., Bromley S.T, Hamad S., Mora-Fonz M., Sokol A.A, and Woodey S.M 2010, PCCP 12, 786-811
Plane J.M.C. 2013, Phil. Trans. R. Soc. A 371 (1994), 20120335
Pont F., Sing D.K., Gibson N.P., Aigrain S., Henry G., Husnoo N. 2013, MNRAS 432, 2917
Sing D.K., Pont F., Aigrain S., Charbonneau D., Desert J.-M. et al. 2011, MNRAS 416, 1443
Sing D.K., Lecavelier des Etangs A., Fortney J.J., Burrows A.S., Pont F. et al. 2013, MNRAS 436, 2956
Schlawin E., Zhao M., Teske J.K., Herter T. 2014, ApJ 783, 5
Syzgantseva O.A, Gonzalez-Navarrete P., Calatayud M., Bromley S.T, and Minot C. 2011, J.Phys. Chem. C, 115(32), 15890-15899
Wetzel S., Klevenz M., Gail H.-P., Pucci A., Trieloff M. 2012, A&A 2013, 553, 92
Witte S., Helling Ch., Hauschildt P. 2009, A&A 506, 1367
Woitke P., Helling C., 2003, A&A, 399, 297
Woitke P., Helling C., 2004, A&A, 414, 335
Gaussian 09, Frisch et al, Gaussian, Inc., Wallingford CT, 2009.
Lee C., Yang W., Parr R.G 1988, Phys. Rev. B 37 785-789

Appendix A: Energy Tables

In the following tables **'Jeong's Geometry'** or similar refers to the original geometries found in Jeong et al. (2000) and **'Bromley's Geometry'** or similar refers to the current (2012) most stable $(TiO_2)_N$ cluster geometries.

Molecule	Sym.	E_0[Hartree]	$E_{\rm zpe}$[eV]	D_{at}[eV]	D_0[eV]	D_0^{exp} [eV]
Ti(^{3}F)	-	-849.299325	0.00	-	-	-
O(^{3}P)	-	-75.060623	0.00	-	-	-
TiO_2	C_{2v}	-999.963285	0.15	12.57	12.42	13.06
$(TiO_2)_2$	C_{2h}	-2000.124814	0.40	30.64	30.24	31.27 ± 0.68
$(TiO_2)_3$	C_2	-3000.269292	0.63	48.22	47.59	
$(TiO_2)_{3\ Bromley}$	C_s	-3000.287915	0.63	48.73	48.10	
$(TiO_2)_4$	C_{2h}	-4000.417659	0.86	65.91	65.05	
$(TiO_2)_{4\ Bromley}$	C_{2v}	-4000.463105	0.87	67.15	66.28	
$(TiO_2)_5$	C_2	-5000.564391	1.09	83.55	82.46	
$(TiO_2)_{5\ Bromley}$	C_s	-5000.632153	1.11	85.41	84.30	
$(TiO_2)_6$	C_{2h}	-6000.711386	1.32	101.20	99.88	
$(TiO_2)_{6\ Bromley}$	C_2	-6000.837167	1.34	104.64	103.30	
$(TiO_2)_{7\ Bromley}$	C_s	-7001.011900	1.58	123.06	121.48	
$(TiO_2)_{8\ Bromley}$	C_{2h}	-8001.195277	1.82	141.71	139.89	
$(TiO_2)_{9\ Bromley}$	C_s	-9001.372943	2.05	160.19	158.14	
$(TiO_2)_{10\ Bromley}$	C_1	-10001.567429	2.27	179.13	176.86	

Table A.1. DFT/B3LYP energies for Ti, O, and $(TiO_2)_n$. E_0 is the internal energy; $E_{\rm zpe}$ is the zero-point energy; D_{at} atomization energy; D_0 atomization energy minus $E_{\rm zpe}$; and $D_0^{\rm exp}$ the expected experimental results.

Molecule	D_0(n) [eV]	D_0(n)/n [eV]	ΔE(n) [eV]	D_0(n)/(x + y) [eV]
TiO_2	12.42	12.42	12.42	4.14
$(TiO_2)_2$	30.24	15.12	18.00	5.04
$(TiO_2)_3$	47.59	15.86	17.35	5.29
$(TiO_2)_{3\ Bromley}$	48.10	16.03	17.86	5.34
$(TiO_2)_4$	65.05	16.26	17.46	5.42
$(TiO_2)_{4\ Bromley}$	66.28	16.57	18.18	5.52
$(TiO_2)_5$	82.46	16.49	17.41	5.50
$(TiO_2)_{5\ Bromley}$	84.30	16.86	18.02	5.62
$(TiO_2)_6$	99.88	16.65	17.42	5.55
$(TiO_2)_{6\ Bromley}$	103.30	17.22	19.00	5.74
$(TiO_2)_{7\ Bromley}$	121.48	17.35	18.18	5.78
$(TiO_2)_{8\ Bromley}$	139.89	17.49	18.41	5.83
$(TiO_2)_{9\ Bromley}$	158.14	17.57	18.25	5.86
$(TiO_2)_{10\ Bromley}$	176.86	17.69	18.72	5.90

Table A.2. Binding energies for $(TiO_2)_n$ clusters. Total binding energy D_0(n), binding per monomer D_0(n)/n, energy gain ΔE(n) by adding a monomer, and the binding energy per atom D_0(n)/(x + y). Bromley energies have larger binding energies that the original Jeong geometries.

Element	$\Delta_f H^\circ(X, 0K)$	$H^\circ(298K) - H^\circ(0K)$	$S^\circ(298K)$
Ti	112.5525812	1.154397705	7.351578203
O	58.98422559	1.037643403	24.51565487

Table A.3. Chemical information on the atoms Ti and O. Note: These values are in *kcal mol*$^{-1}$, *kcal mol*$^{-1}$, and *cal* $K^{-1}mol^{-1}$, respectively. JANAF thermochemical tables (O 1982, Ti 1979)

Appendix B: Thermochemical Tables of $(TiO_2)_N$

Table B.1. The calculated thermochemical values of TiO_2

T K	S° $Jmol^{-1}K^{-1}$	$[-G^\circ - H^\circ(T_r)]/T$ $Jmol^{-1}K^{-1}$	$H^\circ - H^\circ(T_r)$ $kJmol^{-1}$	$\Delta_f H^\circ$ $kJmol^{-1}$	$\Delta_f G^\circ$ $kJmol^{-1}$
0	0.000	Infinite	-10.951	-233.980	-233.980
100	216.499	290.042	-7.606	-234.100	-237.593
200	241.559	259.146	-3.967	-235.289	-240.659
298.15	257.636	255.419	0.000	-236.542	-243.021
300	257.903	255.423	0.079	-236.564	-243.062
400	270.656	257.122	4.521	-237.706	-245.051
500	281.296	260.447	9.294	-238.733	-246.767
600	290.446	264.291	14.317	-239.695	-248.283
700	298.456	268.248	19.515	-240.640	-249.639
800	305.569	272.154	24.842	-241.574	-250.861
900	311.956	275.932	30.267	-242.546	-251.964
1000	317.743	279.558	35.759	-243.637	-252.954
1100	323.030	283.021	41.307	-244.913	-253.825
1200	327.894	286.329	46.897	-250.368	-254.454
1300	332.396	289.484	52.520	-251.307	-254.757
1400	336.580	292.493	58.168	-252.331	-254.981
1500	340.492	295.369	63.839	-253.452	-255.133
1600	344.165	298.123	69.528	-254.685	-255.208
1700	347.624	300.759	75.234	-256.045	-255.201
1800	350.891	303.287	80.949	-257.547	-255.106
1900	353.986	305.714	86.676	-259.209	-254.927
2000	356.929	308.049	92.412	-275.726	-254.199
2100	359.731	310.298	98.154	-278.494	-253.057
2200	362.407	312.465	103.907	-281.273	-251.783
2300	364.965	314.556	109.662	-284.072	-250.377
2400	367.418	316.577	115.425	-286.886	-248.851
2500	369.771	318.531	121.190	-289.720	-247.210
2600	372.034	320.422	126.961	-292.569	-245.450
2700	374.213	322.256	132.735	-295.435	-243.586
2800	376.314	324.033	138.511	-298.321	-241.612
2900	378.343	325.759	144.292	-301.221	-239.534
3000	380.303	327.436	150.074	-304.141	-237.360
3100	382.200	329.067	155.860	-307.073	-235.085
3200	384.038	330.653	161.647	-310.024	-232.717
3300	385.819	332.197	167.436	-312.990	-230.252
3400	387.548	333.702	173.228	-315.970	-227.702
3500	389.227	335.169	179.020	-318.965	-225.061
3600	390.859	336.600	184.814	-321.974	-222.336
3700	392.447	337.998	190.609	-734.096	-211.740
3800	393.993	339.362	196.406	-735.897	-197.595
3900	395.499	340.695	202.205	-737.763	-183.406

Table B.2. The calculated thermochemical values of $(TiO_2)_2$

T K	S° $Jmol^{-1}K^{-1}$	$[-G^\circ - H^\circ(T_r)]/T$ $Jmol^{-1}K^{-1}$	$H^\circ - H^\circ(T_r)$ $kJmol^{-1}$	$\Delta_f H^\circ$ $kJmol^{-1}$	$\Delta_f G^\circ$ $kJmol^{-1}$
0	0.000	Infinite	-18.885	-988.450	-988.450
100	262.813	407.720	-14.845	-991.339	-981.307
200	306.868	345.640	-8.354	-994.505	-969.994
298.15	340.624	337.693	0.000	-996.591	-957.477
300	341.201	337.693	0.173	-996.619	-957.233
400	369.762	341.476	10.129	-997.832	-943.901
500	394.066	348.967	21.036	-998.525	-930.331
600	415.078	357.696	32.567	-998.964	-916.650
700	433.507	366.716	44.526	-999.291	-902.906
800	449.860	375.629	56.776	-999.562	-889.114
900	464.535	384.270	69.237	-999.896	-875.292
1000	477.825	392.566	81.853	-1000.446	-861.419
1100	489.959	400.498	94.584	-1001.363	-847.476
1200	501.116	408.069	107.407	-1010.628	-833.194
1300	511.433	415.292	120.298	-1010.863	-818.397
1400	521.030	422.190	133.247	-1011.258	-803.577
1500	529.994	428.779	146.240	-1011.848	-788.723
1600	538.405	435.084	159.271	-1012.662	-773.828
1700	546.323	441.123	172.333	-1013.730	-758.872
1800	553.804	446.914	185.421	-1015.078	-743.836
1900	560.892	452.475	198.532	-1016.742	-728.726
2000	567.628	457.823	211.663	-1048.120	-712.608
2100	574.042	462.972	224.808	-1051.994	-695.737
2200	580.163	467.934	237.967	-1055.899	-678.684
2300	586.018	472.725	251.140	-1059.835	-661.448
2400	591.629	477.352	264.322	-1063.807	-644.039
2500	597.013	481.827	277.513	-1067.814	-626.473
2600	602.191	486.158	290.714	-1071.853	-608.732
2700	607.176	490.356	303.923	-1075.924	-590.847
2800	611.981	494.427	317.137	-1080.034	-572.807
2900	616.621	498.379	330.359	-1084.174	-554.614
3000	621.106	502.218	343.586	-1088.349	-536.288
3100	625.443	505.950	356.816	-1092.557	-517.814
3200	629.646	509.582	370.051	-1096.798	-499.209
3300	633.720	513.118	383.291	-1101.067	-480.463
3400	637.673	516.562	396.534	-1105.368	-461.595
3500	641.514	519.921	409.783	-1109.692	-442.598
3600	645.246	523.196	423.031	-1114.052	-423.477
3700	648.877	526.394	436.285	-1936.630	-388.659
3800	652.412	529.517	449.541	-1938.570	-346.790
3900	655.857	532.568	462.799	-1940.643	-304.876

Table B.3. The calculated thermochemical values of **Jeong's** $(TiO_2)_3$

T K	S° $Jmol^{-1}K^{-1}$	$[-G^\circ - H^\circ(T_r)]/T$ $Jmol^{-1}K^{-1}$	$H^\circ - H^\circ(T_r)$ $kJmol^{-1}$	$\Delta_f H^\circ$ $kJmol^{-1}$	$\Delta_f G^\circ$ $kJmol^{-1}$
0	0.000	Infinite	-28.116	-1698.152	-1698.152
100	302.773	526.126	-22.792	-1703.223	-1679.030
200	369.250	430.378	-12.973	-1707.887	-1652.910
298.15	421.656	418.028	0.000	-1710.575	-1625.285
300	422.539	418.019	0.268	-1710.610	-1624.752
400	467.293	423.942	15.869	-1711.761	-1595.926
500	505.445	435.685	32.989	-1712.040	-1566.923
600	538.433	449.375	51.095	-1711.890	-1537.909
700	567.344	463.526	69.857	-1711.557	-1508.938
800	592.985	477.510	89.065	-1711.132	-1480.016
900	615.980	491.062	108.591	-1710.797	-1451.151
1000	636.802	504.074	128.353	-1710.784	-1422.308
1100	655.800	516.509	148.288	-1711.321	-1393.438
1200	673.261	528.378	168.358	-1724.383	-1364.136
1300	689.412	539.701	188.535	-1723.895	-1334.137
1400	704.423	550.508	208.793	-1723.653	-1304.160
1500	718.449	560.835	229.119	-1723.702	-1274.201
1600	731.604	570.711	249.504	-1724.084	-1244.227
1700	743.988	580.169	269.933	-1724.850	-1214.217
1800	755.687	589.239	290.401	-1726.036	-1184.139
1900	766.772	597.950	310.901	-1727.700	-1153.998
2000	777.301	606.324	331.430	-1773.933	-1122.384
2100	787.329	614.386	351.982	-1778.910	-1089.683
2200	796.900	622.157	372.556	-1783.933	-1056.754
2300	806.053	629.654	393.150	-1789.001	-1023.580
2400	814.825	636.898	413.758	-1794.124	-990.189
2500	823.242	643.902	434.378	-1799.300	-956.593
2600	831.336	650.683	455.015	-1804.524	-922.773
2700	839.127	657.253	475.659	-1809.800	-888.765
2800	846.639	663.625	496.314	-1815.131	-854.558
2900	853.890	669.808	516.979	-1820.509	-820.149
3000	860.899	675.816	537.652	-1825.938	-785.567
3100	867.679	681.657	558.331	-1831.417	-750.798
3200	874.247	687.339	579.017	-1836.945	-715.854
3300	880.615	692.871	599.711	-1842.515	-680.723
3400	886.793	698.260	620.408	-1848.135	-645.440
3500	892.795	703.514	641.113	-1853.788	-609.983
3600	898.629	708.640	661.820	-1859.493	-574.368
3700	904.303	713.642	682.530	-3092.531	-515.225
3800	909.828	718.527	703.248	-3094.607	-445.532
3900	915.210	723.300	723.966	-3096.887	-375.795

Table B.4. The calculated thermochemical values of **Bromley's** $(TiO_2)_3$

T K	S° $Jmol^{-1}K^{-1}$	$[-G^\circ - H^\circ(T_r)]/T$ $Jmol^{-1}K^{-1}$	$H^\circ - H^\circ(T_r)$ $kJmol^{-1}$	$\Delta_f H^\circ$ $kJmol^{-1}$	$\Delta_f G^\circ$ $kJmol^{-1}$
0	0.000	Infinite	-28.116	-1747.136	-1747.136
100	302.668	526.022	-22.792	-1752.207	-1728.003
200	369.132	430.261	-12.973	-1756.871	-1701.871
298.15	421.551	417.923	0.000	-1759.559	-1674.238
300	422.434	417.914	0.268	-1759.594	-1673.705
400	467.181	423.832	15.869	-1760.745	-1644.865
500	505.335	435.576	32.989	-1761.024	-1615.851
600	538.324	449.266	51.095	-1760.874	-1586.827
700	567.232	463.415	69.857	-1760.541	-1557.843
800	592.877	477.403	89.065	-1760.116	-1528.914
900	615.872	490.955	108.591	-1759.781	-1500.038
1000	636.692	503.965	128.353	-1759.768	-1471.181
1100	655.690	516.401	148.288	-1760.305	-1442.301
1200	673.152	528.269	168.358	-1773.367	-1412.989
1300	689.303	539.593	188.535	-1772.879	-1382.979
1400	704.315	550.400	208.793	-1772.637	-1352.992
1500	718.338	560.726	229.119	-1772.686	-1323.020
1600	731.494	570.602	249.504	-1773.068	-1293.035
1700	743.878	580.060	269.933	-1773.834	-1263.015
1800	755.578	589.131	290.401	-1775.019	-1232.926
1900	766.662	597.842	310.901	-1776.684	-1202.774
2000	777.191	606.215	331.430	-1822.917	-1171.147
2100	787.220	614.278	351.982	-1827.894	-1138.439
2200	796.790	622.048	372.556	-1832.917	-1105.496
2300	805.945	629.546	393.150	-1837.985	-1072.315
2400	814.716	636.790	413.758	-1843.108	-1038.910
2500	823.133	643.794	434.378	-1848.284	-1005.304
2600	831.226	650.574	455.015	-1853.508	-971.471
2700	839.017	657.144	475.659	-1858.784	-937.453
2800	846.530	663.516	496.314	-1864.115	-903.235
2900	853.781	669.700	516.979	-1869.493	-868.815
3000	860.789	675.707	537.652	-1874.922	-834.223
3100	867.570	681.548	558.331	-1880.401	-799.443
3200	874.138	687.231	579.017	-1885.929	-764.488
3300	880.506	692.763	599.711	-1891.499	-729.348
3400	886.685	698.152	620.408	-1897.119	-694.054
3500	892.686	703.406	641.113	-1902.772	-658.583
3600	898.520	708.531	661.820	-1908.477	-622.958
3700	904.194	713.533	682.530	-3141.515	-563.805
3800	909.719	718.419	703.248	-3143.591	-494.102
3900	915.100	723.192	723.966	-3145.871	-424.351

Table B.5. The calculated thermochemical values of **Jeong's** $(TiO_2)_4$

T K	S° $Jmol^{-1}K^{-1}$	$[-G^\circ - H^\circ(T_r)]/T$ $Jmol^{-1}K^{-1}$	$H^\circ - H^\circ(T_r)$ $kJmol^{-1}$	$\Delta_f H^\circ$ $kJmol^{-1}$	$\Delta_f G^\circ$ $kJmol^{-1}$
0	0.000	Infinite	-37.516	-2418.065	-2418.065
100	338.217	639.899	-30.724	-2425.133	-2386.327
200	427.169	510.600	-17.572	-2431.294	-2344.958
298.15	498.118	493.833	0.000	-2434.601	-2301.774
300	499.344	493.841	0.365	-2434.640	-2300.951
400	560.236	501.893	21.595	-2435.747	-2256.171
500	612.225	517.880	44.925	-2435.616	-2211.275
600	657.180	536.525	69.599	-2434.882	-2166.468
700	696.571	555.803	95.161	-2433.892	-2121.812
800	731.500	574.856	121.324	-2432.773	-2077.301
900	762.818	593.316	147.918	-2431.767	-2032.933
1000	791.160	611.036	174.822	-2431.196	-1988.652
1100	817.027	627.976	201.961	-2431.352	-1944.398
1200	840.797	644.140	229.280	-2448.210	-1899.618
1300	862.774	659.559	256.737	-2447.004	-1853.951
1400	883.203	674.274	284.307	-2446.122	-1808.359
1500	902.286	688.334	311.967	-2445.630	-1762.828
1600	920.187	701.782	339.703	-2445.583	-1717.318
1700	937.038	714.659	367.499	-2446.046	-1671.794
1800	952.954	727.008	395.345	-2447.072	-1626.212
1900	968.034	738.866	423.236	-2448.734	-1580.574
2000	982.360	750.265	451.166	-2509.820	-1533.003
2100	996.001	761.239	479.125	-2515.901	-1484.013
2200	1009.021	771.817	507.113	-2522.041	-1434.742
2300	1021.472	782.023	535.124	-2528.245	-1385.174
2400	1033.403	791.882	563.157	-2534.521	-1335.335
2500	1044.855	801.416	591.210	-2540.863	-1285.252
2600	1055.863	810.644	619.277	-2547.277	-1234.887
2700	1066.462	819.586	647.362	-2553.752	-1184.297
2800	1076.680	828.257	675.457	-2560.304	-1133.458
2900	1086.544	836.674	703.566	-2566.920	-1082.375
3000	1096.076	844.849	731.685	-2573.605	-1031.077
3100	1105.299	852.797	759.812	-2580.354	-979.547
3200	1114.233	860.530	787.949	-2587.168	-927.803
3300	1122.894	868.058	816.095	-2594.043	-875.830
3400	1131.298	875.392	844.248	-2600.978	-823.667
3500	1139.460	882.542	872.406	-2607.963	-771.289
3600	1147.394	889.516	900.570	-2615.015	-718.717
3700	1155.113	896.323	928.742	-4258.508	-634.792
3800	1162.627	902.970	956.918	-4260.723	-536.811
3900	1169.947	909.465	985.098	-4263.208	-438.785

Table B.6. The calculated thermochemical values of **Bromley's** $(TiO_2)_4$

T K	S° $Jmol^{-1}K^{-1}$	$[-G^\circ - H^\circ(T_r)]/T$ $Jmol^{-1}K^{-1}$	$H^\circ - H^\circ(T_r)$ $kJmol^{-1}$	$\Delta_f H^\circ$ $kJmol^{-1}$	$\Delta_f G^\circ$ $kJmol^{-1}$
0	0.000	Infinite	-35.788	-2537.384	-2537.384
100	308.759	607.077	-30.359	-2545.814	-2504.063
200	394.258	478.350	-17.649	-2552.416	-2459.498
298.15	465.492	461.487	0.000	-2555.647	-2413.092
300	466.726	461.496	0.368	-2555.684	-2412.209
400	528.034	469.604	21.742	-2556.646	-2364.189
500	580.309	485.698	45.198	-2556.389	-2316.090
600	625.442	504.448	69.970	-2555.558	-2268.102
700	664.942	523.821	95.602	-2554.497	-2220.276
800	699.952	542.957	121.826	-2553.318	-2172.607
900	731.321	561.488	148.464	-2552.267	-2125.085
1000	759.707	579.272	175.407	-2551.656	-2077.659
1100	785.602	596.265	202.578	-2551.781	-2030.260
1200	809.393	612.475	229.923	-2568.613	-1982.337
1300	831.391	627.938	257.404	-2567.383	-1933.533
1400	851.836	642.692	284.993	-2566.483	-1884.806
1500	870.931	656.783	312.671	-2565.973	-1836.137
1600	888.838	670.259	340.420	-2565.912	-1787.490
1700	905.699	683.164	368.229	-2566.363	-1738.834
1800	921.622	695.536	396.088	-2567.375	-1690.116
1900	936.706	707.415	423.989	-2569.026	-1641.344
2000	951.036	718.835	451.925	-2630.107	-1590.643
2100	964.682	729.827	479.894	-2636.177	-1538.521
2200	977.706	740.421	507.890	-2642.310	-1486.118
2300	990.160	750.642	535.909	-2648.506	-1433.417
2400	1002.094	760.515	563.949	-2654.774	-1380.446
2500	1013.548	770.062	592.006	-2661.114	-1327.234
2600	1024.559	779.303	620.080	-2667.519	-1273.739
2700	1035.159	788.255	648.168	-2673.992	-1220.017
2800	1045.379	796.937	676.271	-2680.537	-1166.048
2900	1055.244	805.364	704.382	-2687.149	-1111.836
3000	1064.777	813.549	732.504	-2693.832	-1057.408
3100	1074.003	821.506	760.639	-2700.573	-1002.749
3200	1082.937	829.247	788.779	-2707.385	-947.875
3300	1091.599	836.783	816.927	-2714.257	-892.773
3400	1100.004	844.124	845.083	-2721.189	-837.480
3500	1108.167	851.281	873.244	-2728.172	-781.972
3600	1116.103	858.262	901.413	-2735.219	-726.270
3700	1123.822	865.075	929.587	-4378.709	-639.216
3800	1131.337	871.728	957.764	-4380.924	-538.108
3900	1138.657	878.228	985.946	-4383.406	-436.952

Table B.7. The calculated thermochemical values of **Jeong's** $(TiO_2)_5$

T K	S° $Jmol^{-1}K^{-1}$	$[-G^\circ - H^\circ(T_r)]/T$ $Jmol^{-1}K^{-1}$	$H^\circ - H^\circ(T_r)$ $kJmol^{-1}$	$\Delta_f H^\circ$ $kJmol^{-1}$	$\Delta_f G^\circ$ $kJmol^{-1}$
0	0.000	Infinite	-47.010	-3133.685	-3133.685
100	385.397	765.646	-38.689	-3142.690	-3090.446
200	496.994	602.678	-22.183	-3150.324	-3035.010
298.15	586.566	581.519	0.000	-3154.241	-2977.448
300	588.103	581.516	0.462	-3154.284	-2976.349
400	665.170	591.713	27.329	-3155.337	-2916.817
500	731.013	611.949	56.876	-3154.790	-2857.228
600	787.947	635.557	88.125	-3153.466	-2797.832
700	837.816	659.964	120.487	-3151.819	-2738.690
800	882.040	684.087	153.613	-3149.998	-2679.790
900	921.682	707.462	187.272	-3148.324	-2621.124
1000	957.554	729.897	221.322	-3147.189	-2562.613
1100	990.284	751.339	255.666	-3146.965	-2504.173
1200	1020.361	771.802	290.233	-3167.618	-2445.117
1300	1048.166	791.318	324.974	-3165.692	-2384.985
1400	1074.017	809.947	359.856	-3164.170	-2324.984
1500	1098.159	827.743	394.849	-3163.137	-2265.085
1600	1120.803	844.761	429.936	-3162.660	-2205.240
1700	1142.122	861.061	465.099	-3162.821	-2145.408
1800	1162.256	876.689	500.326	-3163.685	-2085.523
1900	1181.331	891.694	535.607	-3165.344	-2025.593
2000	1199.453	906.121	570.936	-3241.285	-1963.271
2100	1216.709	920.008	606.304	-3248.467	-1899.194
2200	1233.178	933.393	641.706	-3255.725	-1834.784
2300	1248.927	946.307	677.137	-3263.064	-1770.024
2400	1264.018	958.782	712.597	-3270.489	-1704.940
2500	1278.503	970.846	748.078	-3278.003	-1639.572
2600	1292.427	982.523	783.580	-3285.601	-1573.871
2700	1305.832	993.836	819.101	-3293.280	-1507.897
2800	1318.757	1004.808	854.640	-3301.051	-1441.632
2900	1331.232	1015.457	890.189	-3308.907	-1375.075
3000	1343.290	1025.801	925.756	-3316.844	-1308.268
3100	1354.955	1035.858	961.332	-3324.864	-1241.184
3200	1366.253	1045.641	996.918	-3332.968	-1173.840
3300	1377.207	1055.166	1032.517	-3341.144	-1106.227
3400	1387.837	1064.444	1068.124	-3349.397	-1038.389
3500	1398.161	1073.490	1103.739	-3357.712	-970.295
3600	1408.196	1082.314	1139.362	-3366.109	-901.967
3700	1417.959	1090.925	1174.992	-5420.059	-794.461
3800	1427.462	1099.335	1210.628	-5422.413	-669.399
3900	1436.720	1107.551	1246.270	-5425.102	-544.289

Table B.8. The calculated thermochemical values of **Bromley's** $(TiO_2)_5$

T K	S° $Jmol^{-1}K^{-1}$	$[-G^\circ - H^\circ(T_r)]/T$ $Jmol^{-1}K^{-1}$	$H^\circ - H^\circ(T_r)$ $kJmol^{-1}$	$\Delta_f H^\circ$ $kJmol^{-1}$	$\Delta_f G^\circ$ $kJmol^{-1}$
0	0.000	Infinite	-44.169	-3311.595	-3311.595
100	327.321	701.588	-38.036	-3322.786	-3264.734
200	433.260	539.830	-22.251	-3331.142	-3203.082
298.15	523.066	518.565	0.000	-3334.991	-3139.266
300	524.619	518.569	0.465	-3335.031	-3138.051
400	602.139	528.820	27.492	-3335.924	-3072.192
500	668.268	549.172	57.165	-3335.251	-3006.317
600	725.382	572.892	88.511	-3333.830	-2940.657
700	775.363	597.397	120.946	-3332.109	-2875.263
800	819.661	621.607	154.127	-3330.233	-2810.122
900	859.352	645.053	187.831	-3328.515	-2745.218
1000	895.264	667.553	221.918	-3327.343	-2680.477
1100	928.023	689.052	256.291	-3327.090	-2615.812
1200	958.119	709.560	290.882	-3347.719	-2550.528
1300	985.946	729.121	325.646	-3345.770	-2484.176
1400	1011.808	747.784	360.547	-3344.229	-2417.951
1500	1035.961	765.613	395.555	-3343.181	-2351.832
1600	1058.615	782.662	430.655	-3342.690	-2285.770
1700	1079.831	798.879	465.832	-3342.839	-2219.531
1800	1100.080	814.638	501.069	-3343.692	-2153.613
1900	1119.162	829.666	536.361	-3345.340	-2087.468
2000	1137.286	844.112	571.697	-3421.273	-2018.926
2100	1154.547	858.018	607.073	-3428.447	-1948.635
2200	1171.018	871.419	642.481	-3435.700	-1878.008
2300	1186.771	884.349	677.920	-3443.031	-1807.033
2400	1201.859	896.838	713.369	-3450.467	-1735.735
2500	1216.352	908.915	748.871	-3457.960	-1664.152
2600	1230.275	920.604	784.371	-3465.560	-1592.233
2700	1243.686	931.929	819.904	-3473.227	-1520.048
2800	1256.611	942.911	855.446	-3480.995	-1447.568
2900	1269.088	953.570	891.003	-3488.843	-1374.794
3000	1281.146	963.923	926.570	-3496.780	-1301.773
3100	1292.813	973.989	962.151	-3504.795	-1228.474
3200	1304.113	983.780	997.742	-3512.893	-1154.918
3300	1315.068	993.313	1033.344	-3521.067	-1081.090
3400	1325.699	1002.599	1068.954	-3529.317	-1007.040
3500	1336.023	1011.651	1104.571	-3537.629	-932.730
3600	1346.059	1020.481	1140.197	-3546.024	-858.190
3700	1355.822	1029.099	1175.830	-5599.971	-744.469
3800	1365.327	1037.515	1211.469	-5602.322	-613.195
3900	1374.585	1045.737	1247.112	-5605.009	-481.871

Table B.9. The calculated thermochemical values of **Jeong's** $(TiO_2)_6$

T K	S° $Jmol^{-1}K^{-1}$	$[-G^\circ - H^\circ(T_r)]/T$ $Jmol^{-1}K^{-1}$	$H^\circ - H^\circ(T_r)$ $kJmol^{-1}$	$\Delta_f H^\circ$ $kJmol^{-1}$	$\Delta_f G^\circ$ $kJmol^{-1}$
0	0.000	Infinite	-56.566	-3849.996	-3849.996
100	428.245	887.254	-46.671	-3860.891	-3794.774
200	562.553	690.552	-26.798	-3869.986	-3724.842
298.15	670.742	664.971	0.000	-3874.508	-3652.477
300	672.618	664.974	0.562	-3874.552	-3651.098
400	765.871	677.310	33.073	-3875.544	-3576.387
500	845.574	701.807	68.838	-3874.580	-3501.686
600	914.488	730.381	106.661	-3872.667	-3427.277
700	974.844	759.919	145.831	-3870.355	-3353.226
800	1028.359	789.117	185.914	-3867.837	-3279.517
900	1076.324	817.403	226.644	-3865.490	-3206.124
1000	1119.723	844.553	267.840	-3863.791	-3132.958
1100	1159.323	870.505	309.389	-3863.187	-3059.917
1200	1195.705	895.264	351.205	-3887.635	-2986.160
1300	1229.346	918.883	393.234	-3884.984	-2911.145
1400	1260.613	941.424	435.426	-3882.824	-2836.311
1500	1289.815	962.955	477.754	-3881.247	-2761.622
1600	1317.207	983.548	520.195	-3880.338	-2687.024
1700	1342.989	1003.267	562.726	-3880.198	-2612.456
1800	1367.343	1022.175	605.333	-3880.899	-2537.848
1900	1390.415	1040.331	648.005	-3882.555	-2463.207
2000	1412.331	1057.785	690.732	-3973.352	-2385.710
2100	1433.200	1074.585	733.507	-3981.637	-2306.123
2200	1453.119	1090.778	776.323	-3990.012	-2226.155
2300	1472.168	1106.402	819.177	-3998.483	-2145.782
2400	1490.420	1121.494	862.062	-4007.060	-2065.036
2500	1507.937	1136.088	904.973	-4015.743	-1983.960
2600	1524.777	1150.214	947.910	-4024.525	-1902.496
2700	1540.989	1163.900	990.869	-4033.407	-1820.723
2800	1556.619	1177.172	1033.846	-4042.402	-1738.611
2900	1571.707	1190.054	1076.843	-4051.490	-1656.158
3000	1586.289	1202.568	1119.854	-4060.685	-1573.419
3100	1600.397	1214.732	1162.881	-4069.973	-1490.354
3200	1614.061	1226.566	1205.918	-4079.364	-1406.996
3300	1627.309	1238.089	1248.969	-4088.843	-1323.322
3400	1640.165	1249.313	1292.032	-4098.412	-1239.389
3500	1652.650	1260.254	1335.103	-4108.057	-1155.155
3600	1664.786	1270.928	1378.183	-4117.801	-1070.654
3700	1676.592	1281.344	1421.272	-6582.208	-939.146
3800	1688.085	1291.516	1464.367	-6584.701	-786.581
3900	1699.282	1301.455	1507.473	-6587.591	-633.968

Table B.10. The calculated thermochemical values of **Bromley's** $(TiO_2)_6$

T K	S° $Jmol^{-1}K^{-1}$	$[-G^\circ - H^\circ(T_r)]/T$ $Jmol^{-1}K^{-1}$	$H^\circ - H^\circ(T_r)$ $kJmol^{-1}$	$\Delta_f H^\circ$ $kJmol^{-1}$	$\Delta_f G^\circ$ $kJmol^{-1}$
0	0.000	Infinite	-53.636	-4180.234	-4180.234
100	346.986	805.262	-46.526	-4193.914	-4119.672
200	477.697	607.766	-27.069	-4203.425	-4041.310
298.15	586.971	581.920	0.000	-4207.676	-3960.669
300	588.865	581.932	0.564	-4207.717	-3959.137
400	682.794	594.355	33.312	-4208.473	-3876.085
500	762.844	619.008	69.232	-4207.354	-3793.095
600	831.946	647.730	107.157	-4205.339	-3710.424
700	892.411	677.396	146.395	-4202.959	-3628.126
800	945.994	706.696	186.531	-4200.389	-3546.176
900	994.002	735.073	227.295	-4198.007	-3464.552
1000	1037.435	762.296	268.523	-4196.277	-3383.155
1100	1077.054	788.310	310.093	-4195.651	-3301.886
1200	1113.455	813.123	351.930	-4220.078	-3219.903
1300	1147.107	836.789	393.972	-4217.414	-3136.665
1400	1178.382	859.369	436.177	-4215.241	-3053.605
1500	1207.595	880.937	478.518	-4213.651	-2970.696
1600	1234.991	901.562	520.967	-4212.734	-2887.875
1700	1260.779	921.309	563.506	-4212.586	-2805.086
1800	1285.137	940.243	606.120	-4213.280	-2722.258
1900	1308.212	958.420	648.800	-4214.927	-2639.394
2000	1330.131	975.894	691.533	-4305.719	-2553.676
2100	1351.003	992.715	734.313	-4313.999	-2465.871
2200	1370.924	1008.924	777.135	-4322.369	-2377.683
2300	1389.976	1024.565	819.993	-4330.834	-2289.092
2400	1408.228	1039.671	862.881	-4339.409	-2200.126
2500	1425.747	1054.278	905.797	-4348.086	-2110.829
2600	1442.589	1068.417	948.737	-4356.866	-2021.148
2700	1458.802	1082.115	991.698	-4365.745	-1931.156
2800	1474.433	1095.398	1034.678	-4374.738	-1840.824
2900	1489.522	1108.290	1077.678	-4383.824	-1750.153
3000	1504.105	1120.814	1120.692	-4393.016	-1659.197
3100	1518.213	1132.987	1163.719	-4402.303	-1567.914
3200	1531.878	1144.829	1206.761	-4411.689	-1476.335
3300	1545.126	1156.359	1249.814	-4421.166	-1384.441
3400	1557.982	1167.591	1292.877	-4430.734	-1292.290
3500	1570.467	1178.539	1335.949	-4440.379	-1199.839
3600	1582.604	1189.219	1379.033	-4450.119	-1107.117
3700	1594.411	1199.641	1422.123	-6914.525	-967.391
3800	1605.904	1209.820	1465.220	-6917.016	-806.608
3900	1617.101	1219.765	1508.326	-6919.906	-645.777

Table B.11. The calculated thermochemical values of **Bromley's** $(TiO_2)_7$

T K	S° $Jmol^{-1}K^{-1}$	$[-G^\circ - H^\circ(T_r)]/T$ $Jmol^{-1}K^{-1}$	$H^\circ - H^\circ(T_r)$ $kJmol^{-1}$	$\Delta_f H^\circ$ $kJmol^{-1}$	$\Delta_f G^\circ$ $kJmol^{-1}$
0	0.000	Infinite	-61.739	-4969.371	-4969.371
100	369.513	898.759	-53.705	-4985.592	-4895.446
200	518.536	670.197	-31.495	-4997.179	-4800.289
298.15	645.627	640.072	0.000	-5002.223	-4702.369
300	647.833	640.081	0.659	-5002.271	-4700.509
400	757.877	654.632	39.025	-5002.993	-4599.720
500	851.828	683.529	81.183	-5001.435	-4499.055
600	932.963	717.214	125.714	-4998.799	-4398.814
700	1003.969	752.025	171.792	-4995.723	-4299.061
800	1066.875	786.410	218.912	-4992.430	-4199.754
900	1123.238	819.711	266.772	-4989.349	-4100.863
1000	1174.221	851.664	315.165	-4987.036	-4002.275
1100	1220.726	882.197	363.960	-4986.009	-3903.862
1200	1263.445	911.320	413.059	-5014.218	-3804.644
1300	1302.939	939.096	462.400	-5010.818	-3703.986
1400	1339.642	965.598	511.930	-5007.992	-3603.559
1500	1373.922	990.912	561.615	-5005.851	-3503.328
1600	1406.068	1015.117	611.426	-5004.494	-3403.218
1700	1436.331	1038.294	661.342	-5004.033	-3303.167
1800	1464.911	1060.515	711.345	-5004.556	-3203.083
1900	1491.984	1081.847	761.421	-5006.196	-3102.974
2000	1517.703	1102.356	811.560	-5111.835	-2999.553
2100	1542.192	1122.094	861.755	-5121.211	-2893.707
2200	1565.565	1141.118	911.996	-5130.693	-2787.432
2300	1587.916	1159.472	962.277	-5140.290	-2680.695
2400	1609.331	1177.199	1012.595	-5150.012	-2573.536
2500	1629.885	1194.341	1062.947	-5159.853	-2466.002
2600	1649.644	1210.932	1113.325	-5169.815	-2358.031
2700	1668.665	1227.007	1163.726	-5179.893	-2249.708
2800	1687.004	1242.594	1214.152	-5190.102	-2140.998
2900	1704.705	1257.722	1264.596	-5200.425	-2031.906
3000	1721.814	1272.417	1315.060	-5210.867	-1922.486
3100	1738.366	1286.702	1365.541	-5221.420	-1812.697
3200	1754.397	1300.599	1416.034	-5232.092	-1702.573
3300	1769.939	1314.128	1466.541	-5242.870	-1592.087
3400	1785.022	1327.307	1517.064	-5253.752	-1481.311
3500	1799.669	1340.154	1567.594	-5264.723	-1370.193
3600	1813.907	1352.685	1618.135	-5275.811	-1258.767
3700	1827.757	1364.915	1668.686	-8150.672	-1092.511
3800	1841.241	1376.858	1719.248	-8153.296	-901.696
3900	1854.376	1388.527	1769.815	-8156.391	-710.831

Table B.12. The calculated thermochemical values of **Bromley's** $(TiO_2)_8$

T K	S° $Jmol^{-1}K^{-1}$	$[-G^\circ - H^\circ(T_r)]/T$ $Jmol^{-1}K^{-1}$	$H^\circ - H^\circ(T_r)$ $kJmol^{-1}$	$\Delta_f H^\circ$ $kJmol^{-1}$	$\Delta_f G^\circ$ $kJmol^{-1}$
0	0.000	Infinite	-70.471	-5781.203	-5781.203
100	385.397	992.932	-61.615	-5800.067	-5693.352
200	556.199	730.611	-36.151	-5813.226	-5580.927
298.15	702.091	696.050	0.000	-5818.836	-5465.481
300	704.623	696.053	0.759	-5818.885	-5463.286
400	830.859	712.748	44.770	-5819.546	-5344.548
500	938.627	745.900	93.126	-5817.589	-5225.994
600	1031.694	784.543	144.206	-5814.390	-5107.963
700	1113.133	824.468	197.057	-5810.683	-4990.516
800	1185.301	863.912	251.113	-5806.714	-4873.611
900	1249.962	902.113	306.018	-5802.986	-4757.210
1000	1308.454	938.768	361.539	-5800.128	-4641.175
1100	1361.811	973.793	417.523	-5798.737	-4525.362
1200	1410.825	1007.202	473.858	-5830.754	-4408.649
1300	1456.140	1039.067	530.472	-5826.644	-4290.310
1400	1498.256	1069.472	587.303	-5823.188	-4172.253
1500	1537.585	1098.511	644.311	-5820.517	-4054.431
1600	1574.473	1126.282	701.465	-5818.738	-3936.768
1700	1609.195	1152.871	758.741	-5817.983	-3819.182
1800	1641.989	1178.365	816.116	-5818.352	-3701.575
1900	1673.057	1202.840	873.577	-5819.994	-3583.954
2000	1702.567	1226.369	931.110	-5940.494	-3462.555
2100	1730.669	1249.016	988.708	-5950.976	-3338.402
2200	1757.488	1270.841	1046.359	-5961.581	-3213.763
2300	1783.137	1291.900	1104.057	-5972.315	-3088.613
2400	1807.709	1312.239	1161.794	-5983.194	-2962.988
2500	1831.294	1331.907	1219.571	-5994.209	-2836.945
2600	1853.967	1350.943	1277.379	-6005.361	-2710.410
2700	1875.795	1369.386	1335.216	-6016.643	-2583.482
2800	1896.839	1387.271	1393.080	-6028.076	-2456.124
2900	1917.152	1404.628	1450.967	-6039.637	-2328.332
3000	1936.784	1421.489	1508.875	-6051.337	-2200.176
3100	1955.777	1437.879	1566.798	-6063.165	-2071.608
3200	1974.174	1453.824	1624.743	-6075.124	-1942.663
3300	1992.008	1469.346	1682.701	-6087.207	-1813.310
3400	2009.315	1484.468	1740.675	-6099.409	-1683.635
3500	2026.123	1499.209	1798.659	-6111.713	-1553.574
3600	1986.305	1457.914	1856.656	-6124.147	-1221.008
3700	2058.356	1527.620	1914.667	-9409.465	-1230.110
3800	2073.828	1541.324	1972.685	-9412.231	-1008.987
3900	2088.901	1554.712	2030.714	-9415.530	-787.814

Table B.13. The calculated thermochemical values of **Bromley's** $(TiO_2)_9$

T K	S° $Jmol^{-1}K^{-1}$	$[-G^\circ - H^\circ(T_r)]/T$ $Jmol^{-1}K^{-1}$	$H^\circ - H^\circ(T_r)$ $kJmol^{-1}$	$\Delta_f H^\circ$ $kJmol^{-1}$	$\Delta_f G^\circ$ $kJmol^{-1}$
0	0.000	Infinite	-77.878	-6578.040	-6578.040
100	405.981	1079.088	-68.247	-6599.595	-6476.782
200	592.208	787.536	-40.433	-6615.232	-6347.192
298.15	755.288	748.789	0.000	-6621.779	-6213.950
300	758.139	748.796	0.853	-6621.835	-6211.418
400	900.586	767.617	50.522	-6622.422	-6074.398
500	1022.480	805.054	105.220	-6619.925	-5937.643
600	1127.792	848.731	163.017	-6615.992	-5801.544
700	1219.931	893.873	222.810	-6611.486	-5666.158
800	1301.549	938.472	283.945	-6606.700	-5531.427
900	1374.650	981.664	346.020	-6602.199	-5397.299
1000	1440.767	1023.110	408.777	-6598.688	-5263.621
1100	1501.058	1062.709	472.039	-6596.843	-5130.219
1200	1556.442	1100.482	535.691	-6632.586	-4995.836
1300	1607.630	1136.502	599.643	-6627.701	-4859.639
1400	1655.201	1170.870	663.837	-6623.556	-4723.781
1500	1699.622	1203.693	728.224	-6620.296	-4588.208
1600	1741.279	1235.079	792.770	-6618.049	-4452.828
1700	1780.489	1265.129	857.446	-6616.957	-4317.552
1800	1817.521	1293.938	922.236	-6617.130	-4182.266
1900	1852.598	1321.594	987.114	-6618.743	-4046.975
2000	1885.919	1348.181	1052.074	-6754.069	-3907.450
2100	1917.646	1373.770	1117.103	-6765.631	-3764.836
2200	1947.924	1398.428	1182.189	-6777.333	-3621.687
2300	1976.878	1422.219	1247.325	-6789.183	-3477.971
2400	2004.619	1445.198	1312.508	-6801.192	-3333.733
2500	2031.245	1467.417	1377.731	-6813.361	-3189.036
2600	2056.840	1488.921	1442.990	-6825.681	-3043.790
2700	2081.481	1509.756	1508.279	-6838.153	-2898.117
2800	2105.234	1529.958	1573.596	-6850.794	-2751.961
2900	2128.164	1549.564	1638.939	-6863.579	-2605.329
3000	2150.324	1568.609	1704.304	-6876.524	-2458.293
3100	2171.763	1587.121	1769.689	-6889.609	-2310.802
3200	2192.529	1605.131	1835.096	-6902.845	-2162.894
3300	2212.660	1622.663	1900.515	-6916.220	-2014.534
3400	2232.195	1639.743	1965.953	-6929.730	-1865.818
3500	2232.468	1656.391	1965.953	-7008.804	-1716.677
3600	2269.609	1672.630	2096.866	-6957.128	-1567.153
3700	2287.548	1688.478	2162.340	-10652.897	-1347.146
3800	2305.012	1703.953	2227.828	-10655.792	-1095.574
3900	2322.026	1719.074	2293.324	-10659.290	-843.954

Table B.14. The calculated thermochemical values of **Bromley's** $(TiO_2)_{10}$

T K	S° $Jmol^{-1}K^{-1}$	$[-G^\circ - H^\circ(T_r)]/T$ $Jmol^{-1}K^{-1}$	$H^\circ - H^\circ(T_r)$ $kJmol^{-1}$	$\Delta_f H^\circ$ $kJmol^{-1}$	$\Delta_f G^\circ$ $kJmol^{-1}$
0	0.000	Infinite	-88.498	-7419.038	-7419.038
100	423.047	1189.738	-77.702	-7442.892	-7303.629
200	638.627	858.999	-45.566	-7459.036	-7157.337
298.15	822.513	815.436	0.000	-7465.671	-7007.549
300	825.711	815.448	0.956	-7465.725	-7004.706
400	984.759	836.484	56.406	-7466.114	-6850.842
500	1120.484	878.242	117.310	-7463.211	-6697.318
600	1237.652	926.913	181.616	-7458.754	-6544.541
700	1340.160	977.199	248.136	-7453.665	-6392.577
800	1430.969	1026.861	316.157	-7448.253	-6241.349
900	1512.317	1074.952	385.232	-7443.149	-6090.806
1000	1585.899	1121.094	455.075	-7439.135	-5940.774
1100	1653.010	1165.178	525.491	-7436.960	-5791.062
1200	1714.655	1207.225	596.343	-7476.548	-5640.265
1300	1771.643	1247.324	667.541	-7470.979	-5487.469
1400	1824.606	1285.584	739.010	-7466.231	-5335.061
1500	1874.066	1322.125	810.699	-7462.462	-5182.980
1600	1920.450	1357.066	882.570	-7459.811	-5031.122
1700	1964.108	1390.519	954.587	-7458.444	-4879.388
1800	2005.346	1422.593	1026.733	-7458.478	-4727.655
1900	2044.409	1453.384	1098.982	-7460.109	-4575.926
2000	2081.514	1482.983	1171.322	-7610.309	-4419.497
2100	2116.848	1511.472	1243.741	-7622.990	-4259.646
2200	2150.567	1538.926	1316.226	-7635.825	-4099.208
2300	2182.813	1565.415	1388.769	-7648.822	-3938.147
2400	2213.710	1591.000	1461.364	-7661.997	-3776.516
2500	2243.362	1615.738	1534.003	-7675.347	-3614.378
2600	2271.869	1639.683	1606.685	-7688.866	-3451.643
2700	2299.311	1662.879	1679.401	-7702.550	-3288.431
2800	2325.770	1685.374	1752.151	-7716.420	-3124.699
2900	2351.308	1707.206	1824.927	-7730.454	-2960.440
3000	2375.989	1728.412	1897.730	-7744.661	-2795.737
3100	2399.868	1749.026	1970.556	-7759.025	-2630.535
3200	2422.996	1769.079	2043.403	-7773.558	-2464.874
3300	2445.419	1788.602	2116.271	-7788.240	-2298.719
3400	2467.177	1807.619	2189.155	-7803.076	-2132.170
3500	2488.308	1826.158	2262.054	-7818.036	-1965.155
3600	2508.849	1844.241	2334.970	-7833.161	-1797.722
3700	2528.831	1861.888	2407.898	-11939.393	-1551.978
3800	2548.284	1879.122	2480.840	-11942.431	-1271.170
3900	2567.123	1895.851	2553.792	-11946.139	-989.881